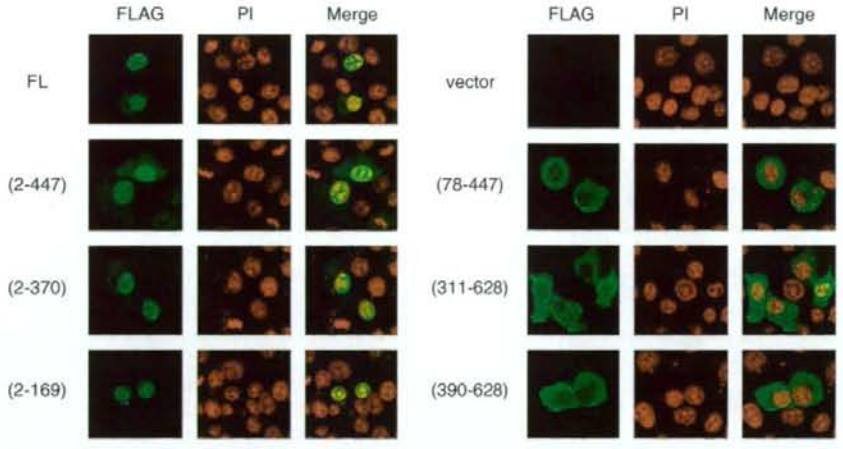

Fig. 3. Subcellular localization of FLAG-tagged deletion mutants of SNARK. Confocal microscopy of PLC/PRF/5 cells expressing FLAG-tagged SNARK deletion mutants showing subcellular localization. Green, wild-type and deletion mutants of SNARK immunostained with anti-FLAG M2 antibody. Red, Nuclei visualized by counter-staining DNA with PI. Original magnification, 630×.

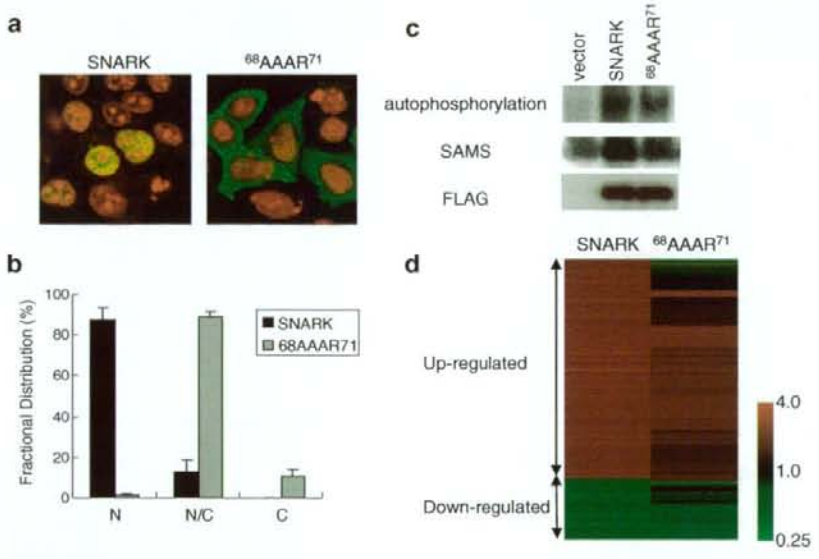

Fig. 4. Identification of a functional NLS in SNARK. (a) Confocal microscopy of cells expressing ^{68}AAAR^{71}-mutant SNARK. Green, wild-type and mutant SNARK immunostained with anti-FLAG M2 antibody. Red, nuclei visualized by counter-staining DNA with PI. Original magnification, 630×. (b) Bar graphs (mean ± SE; $n = 3$) representing the localization of FLAG-SNARK and FLAG-^{68}AAAR^{71} determined in over 300 cells transfected with each plasmid. N; predominantly nuclear localization; N/C, nuclear/cytoplasmic localization; C, predominantly cytoplasmic localization. (c) *In vitro* kinase assay of SNARK or ^{68}AAAR^{71}-mutant SNARK. The PEG precipitants of SNARK and ^{68}AAAR^{71}-mutant SNARK were prepared from lysates of transiently transfected PLC/PRF/5 cells and used to perform a kinase assay with GST-SAMS as substrate. Upper panel indicates an autophosphorylation assay, middle panel indicates *in vitro* kinase assay, and lower panel indicates anti-FLAG immunoblot, respectively. (d) Expression of the probe sets up-regulated more than 1.5-fold and down-regulated less 0.67 by SNARK. Relative expression in the wild-type or ^{68}AAAR^{71}-mutant SNARK expressing cells standardized by the expression in vector-transfected cells was visualized.

whereas GFP without the NLS was distributed in both the nucleus and the cytoplasm (Supplementary Figure 2e).

The NLS motif that we identified above is conserved among all reported orthologs, including those in chimpanzee, cattle, mouse, rat, and chicken (Supplementary Figure 2f).

In these results, SNARK constitutively resided in the nucleus and was activated by AICAR and glucose-deprivation. AICAR and glucose-deprivation increase the cellular AMP:ATP ratio [1]. AMPK and AMPK-related kinases are believed to be activated by increased AMP:ATP ratio through direct activation mechanism of allosteric effect and/or indirectly activated by phosphorylation at threonine residue in the activation loop by upstream kinases, LKB1, CaMKK, and TAK1 [19]. CaMKK and TAK1 are to be localized in the cytoplasm, but LKB1 is localized in both nucleus and cyto-

plasm [20–22]. Therefore SNARK might be phosphorylated by LKB1 in the nucleus. It is possible that SNARK might form a complex with LKB1 or other AMPKK in the nucleus, but this remains to be determined.

The gene expression alterations by overexpressed SNARK

As SNARK was localized in the nucleus, we considered that SNARK might regulate cell cycle or gene expression. There was no significant difference in cell growth between PLC/PRF/5 cells stably expressing SNARK and vector control (data not shown). To evaluate that SNARK modulates gene expression in the nucleus, we compared the gene expression profiles of SNARK overexpressing PLC/PRF/5 cells to NLS mutant SNARK (^{68}AAAR^{71}) expressing PLC/PRF/5 cells and vector-transfected PLC/PRF/5 cells. Among 54,000 probe sets on the HG-U133 Plus 2.0 Affymetrix GeneChip, 20,308 probe sets were assigned for "present" in all the samples from vector, wild-type and ^{68}AAAR^{71}-mutant SNARK transfected cells.

First, to assess whether SNARK modulates gene expression, we compared the expression profiles of SNARK overexpressing cells with those of vector-transfected cells. We identified 945 (739 up-regulated and 206 down-regulated) probe sets with more than 1.5-fold change in expression. This indicated that SNARK altered the gene expression. Second, to identify that SNARK functions as a transcriptional modulator in the nucleus but not the cytoplasm, we examined the expression profiles of ^{68}AAAR^{71} overexpressing cells compared with those of vector-transfected cells (Fig. 4D). Among the 739 up-regulated probe sets by overexpressed SNARK, only 187 probe sets increased more than 1.5-fold in ^{68}AAAR^{71} overexpressing cells. In parallel, among the 206 down-regulated probe sets by overexpressed SNARK, only 67 probe sets decreased more than 1.5-fold in ^{68}AAAR^{71} overexpressing cells. Similarly we identified 108 (76 up-regulated and 32 down-regulated) probe sets with more than 2.0-fold change in SNARK overexpressing cells compared with vector-transfected cells (Supplementary Table 2). Among the 76 up-regulated probe sets by overexpressed SNARK, only eight probe sets increased more than 2.0-fold in ^{68}AAAR^{71} overexpressing cells compared with vector-transfected cells. On the other hand, among the 32 down-regulated probe sets by overexpressed SNARK, only 13 probe sets decreased more than 2.0-fold in ^{68}AAAR^{71} overexpressing cells compared with vector-transfected cells. Thus, overexpressed SNARK altered the gene expression profiles more than ^{68}AAAR^{71}. This result implied that SNARK in the nucleus but not the cytoplasm had a remarkable impact on the gene expression.

In this study, SNARK is localized in the nucleus and affects gene expression profiles. These results indicate that SNARK can work as a transcriptional modulator working in the nucleus in response to stress. Among 76 probe sets with more than 2.0-fold increase in PLC/PRF/5 cells overexpressing SNARK, nine probe sets also detected more than 2.0-fold increase in a human pancreatic cancer cell line PANC-1 under glucose-deprivation (our unpublished data). This concordance of induced genes between the overexpression of SNARK and glucose-deprivation well consists with the activation of SNARK under glucose-deprivation.

The present study demonstrates for the first time, to our knowledge, the alteration of gene expression profiles by SNARK. This information may be the platform to elucidate the molecular mechanism and the physiological signification of SNARK.

Acknowledgments

This work was supported by Grants for the Third-Term Comprehensive 10-Year Strategy for Cancer Control, and a Grant-in-Aid for Cancer Research from the Ministry of Health, Labour and Welfare and a Grant-in-Aid for Scientific Research on Priority Areas from the Ministry of Education, Culture, Sports, Science and Technology, Japan.

Appendix A. Supplementary data

Supplementary data associated with this article can be found, in the online version, at doi:10.1016/j.bbrc.2008.10.143.

References

[1] B.B. Kahn, T. Alquier, D. Carling, D.G. Hardie, AMP-activated protein kinase: ancient energy gauge provides clues to modern understanding of metabolism, Cell Metab. 1 (2005) 15–25.
[2] D.G. Hardie, S.A. Hawley, J.W. Scott, AMP-activated protein kinase—development of the energy sensor concept, J. Physiol. 574 (2006) 7–15.
[3] D.G. Hardie, D. Carling, M. Carlson, The AMP-activated/SNF1 protein kinase subfamily: metabolic sensors of the eukaryotic cell?, Annu Rev. Biochem. 67 (1998) 821–855.
[4] B.E. Kemp, K.I. Mitchelhill, D. Stapleton, B.J. Michell, Z.P. Chen, L.A. Witters, Dealing with energy demand: the AMP-activated protein kinase, Trends Biochem. Sci. 24 (1999) 22–25.
[5] A.M. Turnley, D. Stapleton, R.J. Mann, L.A. Witters, B.E. Kemp, P.F. Bartlett, Cellular distribution and developmental expression of AMP-activated protein kinase isoforms in mouse central nervous system, J. Neurochem. 72 (1999) 1707–1716.
[6] I. Salt, J.W. Celler, S.A. Hawley, A. Prescott, A. Woods, D. Carling, D.G. Hardie, AMP-activated protein kinase: greater AMP dependence, and preferential nuclear localization, of complexes containing the alpha2 isoform, Biochem. J. 334 (Pt. 1) (1998) 177–187.
[7] M. Kodiha, J.G. Rassi, C.M. Brown, U. Stochaj, Localization of AMP kinase is regulated by stress, cell density, and signaling through the MEK–>ERK1/2 pathway, Am. J. Physiol. Cell Physiol. 293 (2007) C1427–C1436.
[8] A. Suzuki, S. Okamoto, S. Lee, K. Saito, T. Shiuchi, Y. Minokoshi, Leptin stimulates fatty acid oxidation and peroxisome proliferator-activated receptor alpha gene expression in mouse C2C12 myoblasts by changing the subcellular localization of the alpha2 form of AMP-activated protein kinase, Mol. Cell. Biol. 27 (2007) 4317–4327.
[9] J.M. Lizcano, O. Goransson, R. Toth, M. Deak, N.A. Morrice, J. Boudeau, S.A. Hawley, L. Udd, T.P. Makela, D.G. Hardie, D.R. Alessi, LKB1 is a master kinase that activates 13 kinases of the AMPK subfamily, including MARK/PAR-1, EMBO J. 23 (2004) 833–843.
[10] G. Manning, D.B. Whyte, R. Martinez, T. Hunter, S. Sudarsanam, The protein kinase complement of the human genome, Science 298 (2002) 1912–1934.
[11] D.L. Lefebvre, Y. Bai, N. Shahmolky, M. Sharma, R. Poon, D.J. Drucker, C.F. Rosen, Identification and characterization of a novel sucrose-non-fermenting protein kinase/AMP-activated protein kinase-related protein kinase, SNARK, Biochem. J. 355 (2001) 297–305.
[12] D.L. Lefebvre, C.F. Rosen, Regulation of SNARK activity in response to cellular stresses, Biochim. Biophys. Acta 1724 (2005) 71–85.
[13] K. Tsuchihara, T. Ogura, R. Fujioka, S. Fujii, W. Kuga, M. Saito, T. Ochiya, A. Ochiai, H. Esumi, Susceptibility of Snark-deficient mice to azoxymethane-induced colorectal tumorigenesis and the formation of aberrant crypt foci, Cancer Sci. 99 (2008) 677–682.
[14] A. Suzuki, G. Kusakai, A. Kishimoto, Y. Minegichi, T. Ogura, H. Esumi, Induction of cell–cell detachment during glucose starvation through F-actin conversion by SNARK, The fourth member of the AMP-activated protein kinase catalytic subunit family, Biochem. Biophys. Res. Commun. 311 (2003) 156–161.
[15] A. Kishimoto, T. Ogura, H. Esumi, A pull-down assay for 5′ AMP-activated protein kinase activity using the GST-fused protein, Mol. Biotechnol. 32 (2006) 17–21.
[16] P. Legembre, R. Schickel, B.C. Barnhart, M.E. Peter, Identification of SNF1/AMP kinase-related kinase as an NF-kappaB-regulated anti-apoptotic kinase involved in CD95-induced motility and invasiveness, J. Biol. Chem. 279 (2004) 46742–46747.
[17] M.R. Hodel, A.H. Corbett, A.E. Hodel, Dissection of a nuclear localization signal, J. Biol. Chem. 276 (2001) 1317–1325.
[18] S.W. Leung, M.T. Harreman, M.R. Hodel, A.E. Hodel, A.H. Corbett, Dissection of the karyopherin alpha nuclear localization signal (NLS)-binding groove: functional requirements for NLS binding, J. Biol. Chem. 278 (2003) 41947–41953.
[19] T. Williams, J.E. Brenman, LKB1 and AMPK in cell polarity and division, Trends Cell Biol. 18 (2008) 193–198.
[20] J. Nezu, A. Oku, M. Shimane, Loss of cytoplasmic retention ability of mutant LKB1 found in Peutz-Jeghers syndrome patients, Biochem. Biophys. Res. Commun. 261 (1999) 750–755.
[21] S.M. Lemrow, K.A. Anderson, J.D. Joseph, T.J. Ribar, P.K. Noeldner, A.R. Means, Catalytic activity is required for calcium/calmodulin-dependent protein kinase IV to enter the nucleus, J. Biol. Chem. 279 (2004) 11664–11671.
[22] K. Deacon, J.L. Blank, Characterization of the mitogen-activated protein kinase kinase 4 (MKK4)/c-Jun NH2-terminal kinase 1 and MKK3/p38 pathways regulated by MEK kinases 2 and 3. MEK kinase 3 activates MKK3 but does not cause activation of p38 kinase in vivo, J. Biol. Chem. 272 (1997) 14489–14496.

TAp73 knockout shows genomic instability with infertility and tumor suppressor functions

Richard Tomasini,[1,2,12] Katsuya Tsuchihara,[1,3,12] Margareta Wilhelm,[1] Masashi Fujitani,[4] Alessandro Rufini,[1,5] Carol C. Cheung,[1,6] Fatima Khan,[7] Annick Itie-Youten,[1] Andrew Wakeham,[1] Ming-sound Tsao,[8] Juan L. Iovanna,[2] Jeremy Squire,[9] Igor Jurisica,[10] David Kaplan,[4] Gerry Melino,[5,11] Andrea Jurisicova,[7] and Tak W. Mak[1,13]

[1]The Campbell Family Institute for Breast Cancer Research, Princess Margaret Hospital, Toronto, Ontario M5G 2C1, Canada; [2]Institut National de la Santé et de la Recherche Médicale Unité 624, Stress Cellulaire, 13288 Marseille Cedex 9, France; [3]Research Center for Innovative Oncology, National Cancer Center Hospital East, Kashiwa, Chiba 277-8577, Japan; [4]The Hospital for Sick Children MaRs Centre, Toronto Medical Discovery Tower, Toronto, Ontario M5G 1L7, Canada; [5]Biochemistry IDI-IRCCS Laboratory, c/o University of Rome "Tor Vergata," 00133 Rome, Italy; [6]Department of Pathology, University Health Network, University of Toronto, Toronto, Ontario M5G 2C4, Canada; [7]Division of Reproductive Endocrinology and Infertility, Department of Obstetrics and Gynecology, Mount Sinai Hospital, Toronto, Ontario M5G 2C1, Canada; [8]Division of Applied Molecular Oncology, Ontario Cancer Institute, Department of Medical Biophysics, University of Toronto, Toronto, Ontario M5G 2C4, Canada; [9]Department of Laboratory Medicine and Pathobiology, University of Toronto, Toronto, Ontario M5G 1L5, Canada; [10]Division of Signaling Biology, Ontario Cancer Institute, Department of Medical Biophysics, University of Toronto, Toronto, Ontario M5G 2C4, Canada; [11]Medical Research Council, Toxicology Unit, Hodgkin Building, Leicester University, Leicester LE1 9HN, United Kingdom

The *Trp53* gene family member *Trp73* encodes two major groups of protein isoforms, TAp73 and ΔNp73, with opposing pro- and anti-apoptotic functions; consequently, their relative ratio regulates cell fate. However, the precise roles of p73 isoforms in cellular events such as tumor initiation, embryonic development, and cell death remain unclear. To determine which aspects of p73 function are attributable to the TAp73 isoforms, we generated and characterized mice in which exons encoding the TAp73 isoforms were specifically deleted to create a TAp73-deficient ($TAp73^{-/-}$) mouse. Here we show that mice specifically lacking in TAp73 isoforms develop a phenotype intermediate between the phenotypes of $Trp73^{-/-}$ and $Trp53^{-/-}$ mice with respect to incidence of spontaneous and carcinogen-induced tumors, infertility, and aging, as well as hippocampal dysgenesis. In addition, cells from $TAp73^{-/-}$ mice exhibit genomic instability associated with enhanced aneuploidy, which may account for the increased incidence of spontaneous tumors observed in these mutants. Hence, TAp73 isoforms exert tumor-suppressive functions and indicate an emerging role for *Trp73* in the maintenance of genomic stability.

[*Keywords*: *p73*; tumor-prone phenotype; meiosis; infertility; genomic instability]

Supplemental material is available at http://www.genesdev.org.

Received May 13, 2008; revised version accepted August 6, 2008.

p73 belongs to a small but important family of p53-related proteins (p53, p63, p73). These proteins, which are encoded by the *Trp53*, *Trp63*, and *Trp73* genes, respectively, are all transcription factors involved in the regulation of development, cell death, proliferation, stem cell renewal, and cell fate commitment, as well as tumorigenesis (Yang et al. 2002; Vousden and Lane 2007). Like p53, several different protein isoforms of p63 and p73 have been reported, whose functions may compete with, synergize with, or be unrelated to those of p53 (Bourdon et al. 2005; Li and Prives 2007).

The *Trp73* gene, discovered in 1997 (Kaghad et al. 1997), contains two promoters that drive the expression of two major groups of p73 isoforms with opposing cellular actions: The TAp73 isoforms contain the p73 transactivation domain (TA) and exhibit proapoptotic activities (Müller et al. 2005; Wang et al. 2007), whereas the ΔNp73 isoforms lacking the N-terminal TA domain are anti-apoptotic (Grob et al. 2001). Consequently, due to the complexity of the cross-talk between all p53 family

[12]These authors contributed equally to this work.
[13]Corresponding author.
E-MAIL tmak@uhnres.utoronto.ca; FAX (416) 204 5300.
Article published online ahead of print. Article and publication date are online at http://www.genesdev.org/cgi/doi/10.1101/gad.1695308. Freely available online through the *Genes & Development* Open Access option.

members and the opposing functions of p73 isoforms harbored in the same gene, the specific role of *Trp73* in various biological processes is still debated (McKeon and Melino 2007; Stiewe 2007).

Mouse gene targeting studies have revealed that both *Trp63* and *Trp73* are required for normal embryogenesis (Mills et al. 1999; Yang et al. 1999, 2000). In contrast, the majority of mice deficient in *Trp53* are viable and appear normal, although ~30% of p53-deficient females die in utero with neuronal defects (Donehower et al. 1992). In addition, *Trp53*$^{-/-}$ mice of both sexes are more susceptible than the wild type to the development of spontaneous tumors (Donehower et al. 1992). In comparison, studies of mice that are homozygous or heterozygous for a complete deletion of *Trp73* have produced conflicting results. Indeed, while inactivation of all p73 isoforms in mice does not enhance susceptibility to spontaneous tumors (Yang et al. 2000), *Trp73* haploinsufficiency contributes to an increased incidence of spontaneous tumors such as lung adenoma, lung adenocarcinoma, thymic lymphoma, squamous cell hyperplasia, or hemangiosarcoma, particularly when combined with *Trp53* heterozygosity (Flores et al. 2005). However, this gene interaction appears to be tissue-specific as *Trp73* does not contribute to *Trp53* tumor suppressor activity during lymphomagenesis (Perez-Losada et al. 2005). It is likely that *Trp73*$^{-/-}$ mouse models do not show enhanced spontaneous tumor formation be due to shortened life span. Despite the fact that studies involving *Trp73*$^{+/-}$ revealed enhanced tumor formation, the *Trp73*$^{-/-}$ mouse model does not seem to fully mirror the molecular changes seen in human cancers, where an altered ratio of TAp73/ΔNp73 isoforms is often present rather than a total loss or mutation of p73 isoforms (Coates 2006). Thus, despite the usefulness of *Trp73*$^{-/-}$ mice, isoform-selective knockouts of *Trp73* are needed to truly evaluate p73's impact on tumorigenesis and other cellular processes.

The complexity of the overlapping, combined, and opposing functions of *Trp53* family members and their protein isoforms suggests the existence of an intricate functional network (Deyoung and Ellisen 2007). Over the last few years, several studies have suggested specific roles for particular p73 isoforms (De Laurenzi et al. 1998; Murray-Zmijewski et al. 2006; Klanrit et al. 2008). Thus, these data indicate that the ratio of various p73 isoforms present in an individual cell determines the outcome of p73 function, rather than the sum of the activities of each isolated p73 isoform. To investigate this hypothesis and elucidate the biological role of TAp73 isoforms, we generated mice that are missing exons encoding the TA domain of p73 (TAp73$^{-/-}$ mice). These mutants are deficient only in TAp73 isoforms and remain capable of producing ΔNp73 isoforms causing a great imbalance in the TAp73/ΔNp73 ratio. We clearly demonstrate that TAp73 isoforms are tumor-suppressive, which may be a consequence of TAp73's apparent role in the maintenance of genomic stability. In addition, we demonstrate that TAp73 is a novel maternal-lethal gene whose deficiency in mice causes infertility, and its loss mimics *Trp73* deficiency causing hypocampal dysgenesis.

Results

Characterization of TAp73 deletion and its effects on the expression and activities of Trp53 family members

To determine the specific role of the TAp73 isoforms of p73 (Fig. 1A), we generated TAp73-deficient mice in which deletion of exons 2 and 3 of the *Trp73* gene (Fig. 1B) selectively abolished expression of all TAp73 isoforms (Supplemental Fig. S1A–C). Firstly, we confirmed the specific deletion of TAp73, and we analyzed the expression patterns of ΔNp73, p53, and p63 in various tissues of TAp73$^{-/-}$ mice. Although p53 and p63 expression were not modified (Supplemental Fig. S2A,D; data not shown), ΔNp73 mRNA was up-regulated in most tissues of TAp73$^{-/-}$ mice (Fig. 1C; Supplemental Fig. S2B). The exception was the lung, where ΔNp73 mRNA was not significantly different from that of wild-type mice (Fig. 1C). We also observed enhanced ΔNp73 mRNA expression in TAp73$^{-/-}$ mouse embryonic fibroblasts (MEFs), and this increased expression was persistent even after the excision of the PGK-neo cassette (Supplemental Fig. S1D,E), indicating that the observed up-regulation of ΔNp73 mRNA is due to the absence of TAp73 proteins rather than to the insertion of the PGK-neo cassette close to the ΔNp73 promoter. However, the enhanced ΔNp73 mRNA level is not reflected in a significant increase in ΔNp73 protein level. Indeed, we analyzed ΔNp73 protein level in lung and ovaries from TAp73$^{-/-}$ tissues versus wild-type tissues by using two antibodies—one specific of the ΔN region (IMG-313) and one specific of the a-C-terminal region from all p73 isoforms (C-17)—and we compared the bands corresponding to the ΔNp73 isoforms (Fig. 1D). Therefore, the antibody data would suggest that the increases in ΔNp73 transcript levels are not accompanied by parallel increases in expression of ΔNp73 protein. The elevated levels of ΔNp73 mRNA in TAp73$^{-/-}$ mice were unexpected because TAp73 is a known transcriptional inducer of ΔNp73 (Grob et al. 2001). However, further examination showed that, in wild-type mice, ΔNp73 levels decreased more rapidly than levels of TAp73 following DNA damage (Maisse et al. 2004; Toh et al. 2004) due to the ubiquitination and proteasomal degradation of ΔNp73 by an as-yet-uncharacterized ubiquitin ligase (B.S. Sayan, C. Piro, A.L. Yang, and G. Melino, unpubl.). These data suggest that there are multiple mechanisms that operate post-transcriptionally to control the levels of various p73 isoforms, resulting in a complex inteplay between TAp73 and ΔNp73. Nonetheless, our TAp73$^{-/-}$ knockout seems to be a pure TAp73-deficient mouse at the protein level, reminiscent of the TAp73/ΔNp73 imbalance observed in human tumors.

Since ΔNp73 is a functional inhibitor of p53 and TAp73 isoforms (Grob et al. 2001; Deyoung and Ellisen 2007), and as we observed an increase in ΔNp73 mRNA level, we wanted to be sure that no ΔNp73 activity was induced, potentially interfering with p53 functions. We showed that p53 activation was comparable in wild-type and TAp73$^{-/-}$ MEFs (Supplemental Fig. S2C,D). Further-

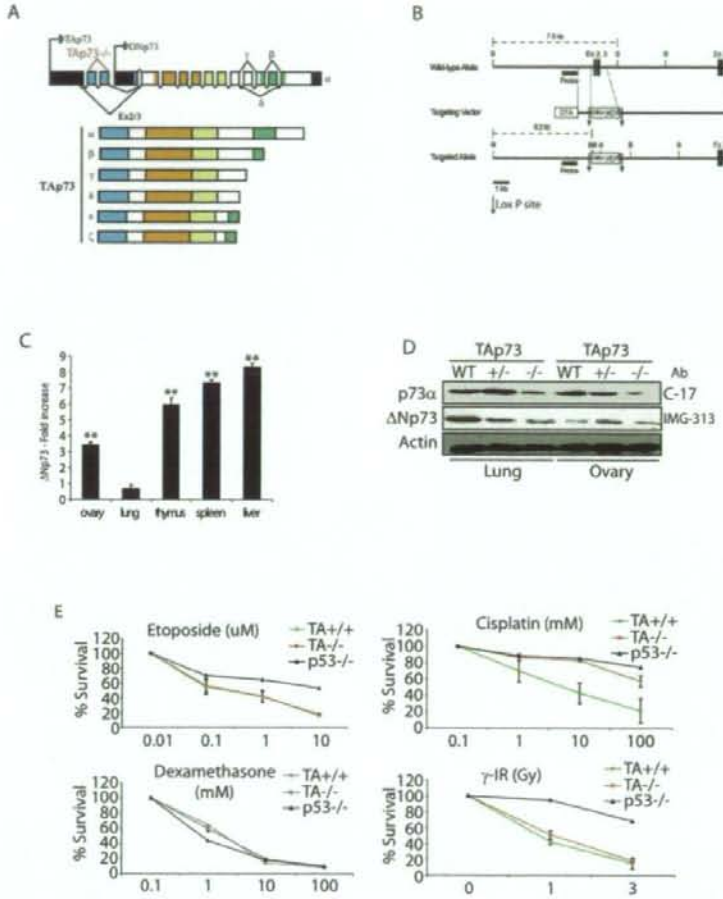

Figure 1. Generation of TAp73$^{-/-}$ mice and up-regulation of ΔNp73 expression. (*A*) Structure of the murine *Trp73* gene showing the TAp73 and ΔNp73 isoform families. Domains: (blue) transactivation; (orange) DNA binding; (yellow) oligomerization; (green) sterile α motif. (*B*) Targeting strategy. Homologous recombination of the indicated targeting vector with the wild-type *Trp73* gene resulted in the replacement of ~1.5 kb with the *neo* gene and the deletion of exons 2 and 3 specific to the TAp73 isoform. LoxP sites and the probe used for Southern blotting are indicated. (*C*) Quantitation of ΔNp73 expression in tissues from TAp73$^{+/+}$ and TAp73$^{-/-}$ mice. Fold increase of ΔNp73 mRNA level in TAp73$^{-/-}$ tissues compared with wild-type tissues by real-time PCR. (**) $P < 0.01$ (Student's *t*-test). (*D*) Western blot analysis of ΔNp73 level in lung and ovary from 10-mo-old wild-type and TAp73-deficient mice. C-17 antibody is specific from α-C-terminal isoforms, and IMG-313 antibody is specific from ΔNp73 isoforms. (Ab) Antibody. (*E*) Thymocyte death. Thymocytes from TAp73$^{+/+}$, TAp73$^{-/-}$, and p53$^{-/-}$ mice were treated for 24 h with the indicated agents at the indicated concentrations, and percent cell death was assayed by annexinV staining and flow cytometry. Data represent the mean ± SD of two experiments.

more, we detected no differences between wild-type and TAp73$^{-/-}$ thymocytes (Fig. 1E), primary MEFs (Supplemental Fig. S2E), or E1A-transformed MEFs (Supplemental Fig. S2F) in p53-dependent cell death induced by γ-irradiation, etoposide, cisplatin, or doxorubicin. The normal sensitivity to death of TAp73$^{-/-}$ thymocytes is particularly interesting in view of the finding that E2F binding to the TAp73 promoter is required for the TCR-induced death of human peripheral T cells from wild-type mice as well as for the death of cancer cells (Irwin et al. 2000; Lissy et al. 2000; Stiewe and Pützer 2000). Our data suggest that the ΔNp73 mRNA increase observed in most tissues from TAp73-deficient mice is not relevant since ΔNp73 protein levels appear normal. A compensatory mechanism may have been elicited in the TAp73-deficient mice to guarantee normal ΔNp73 protein expression under normal or physiological conditions.

Loss of TAp73 leads to infertility due to defects in early embryonic development

A significant percentage of TAp73$^{-/-}$ mice die during embryogenesis, resulting in an abnormal Mendelian ratio at birth (+/+, 29%; +/−, 52%; −/−, 19%) either in mixed or pure background mice (Supplemental Fig. S3A). This partial embryonic lethality could theoretically be caused by the potential enhanced ΔNp73 protein not balanced by the TAp73 at specific stages of embryonic development. Indeed, strongly deregulated ΔNp73 expression in ΔNp73 transgenic mice leads to 100% embryonic lethality partially due to inhibition of p53 activities (Erster et al. 2006; Huttinger-Kirchhof et al. 2006).

We were unable to obtain pups from mating trials involving mating a TAp73$^{-/-}$ male or female with wild-type mice, suggesting that both sexes are infertile (Supplemental Fig. S3B). In contrast to *Trp73*$^{-/-}$ mice, in which defects in sensory and hormonal pathways contribute to reproductive and behavioral phenotypes that lead to male and female infertility, TAp73$^{-/-}$ mice mate normally and the females display normal cyclicity (Supplemental Fig. S3B; data not shown). To investigate the nature of TAp73$^{-/-}$ female infertility, we induced superovulation in 3- to 4-wk-old TAp73$^{-/-}$ females and their wild-type littermate sisters using exogenous gonadotropins. In contrast to wild-type females, no oocytes were present in the fallopian tubes of TAp73$^{-/-}$ females 16 h after administration of hCG (human choriogonadotropin). When the ovaries and oviducts of TAp73$^{-/-}$ females were dissected, we found that the ovulated oocytes were trapped under the bursa and did not progress toward the fallopian tubes (Fig. 2A, right). Upon collection of these oocytes, it became clear that TAp73$^{-/-}$ females also ovulated fewer gametes (Fig. 2B).

To establish if altered follicular development was responsible for the oocyte deficit in TAp73$^{-/-}$ female mice, we performed morphometric analyses (based on the counting of nonatretic follicles) of ovaries obtained from adolescent TAp73$^{+/+}$ and TAp73$^{-/-}$ females. Although significant differences were observed in the number of quiescent (primordial) or early growing (primary) follicles, numbers of early secondary follicles were comparable (Fig. 2C). To examine the later "Graffian follicle" stages, which are dependent on gonadotropins, we treated prepubertal TAp73$^{+/+}$ and TAp73$^{-/-}$ females with a single dose of pregnant mare serum gonadotropin (PMSG) to synchronize follicular development. Ovaries collected 46 h later revealed no significant differences in the competence of TAp73$^{-/-}$ gonads to form large antral ovulatory follicles (Fig. 2D, left). However, when we assessed the ovulatory capacity of these follicles, we found that a greater number of oocytes remained trapped within the luteininzing granulosa cells of TAp73$^{-/-}$ ovaries compared with wild-type females (Fig. 2D, right). To confirm that ΔNp73 was not responsible for that phenotype, we determined that ΔNp73 mRNA expression level was even reduced in MII oocytes from TAp73$^{-/-}$ mice compared with wild-type MII oocytes (Supplemental Fig. S4A). These results suggest that the decreased number of

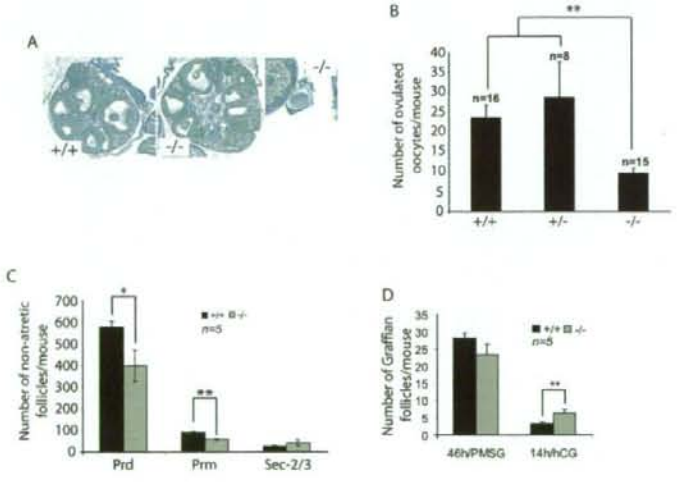

Figure 2. Characterization of reproductive defects in TAp73$^{-/-}$ female mice. (*A*) Normal TAp73$^{-/-}$ ovarian structure. (*Left* and *center* panels) Sections of ovaries from 4-wk-old TAp73$^{+/+}$ and TAp73$^{-/-}$ mice stained with picric acid and methyl blue. Magnification, 5 × 10. (*Right* panel) While no obvious differences in gross ovarian morphology were detected, ovulated oocytes were trapped under the bursa in TAp73$^{-/-}$ ovary. Magnification, 40 × 10. (*B*) TAp73-deficient females ovulate fewer oocytes. Immature TAp73$^{+/+}$, TAp73$^{+/-}$, and TAp73$^{-/-}$ females were superovulated, and the number of oocytes per mouse was counted. The results shown are the mean ovulated oocyte number ± SE for the indicated number (*n*) of mice/genotype. (**) $P < 0.001$ (Student's *t*-test). (*C*) Ovarian reserve is diminished by TAp73 deficiency. Serial sections of ovaries from superovulated immature TAp73$^{+/+}$ and TAp73$^{-/-}$ mice were subjected to histomorphometric analysis. The results shown are the mean number of nonatretic follicles/mouse ± SE for 5 mice per group. (*) $P < 0.01$; (**) $P < 0.001$ (Student's *t*-test). The number of both primordial (Prd) and primary (Prm) follicles is significantly decreased, but the growth rate evidenced by the number of secondary follicles with two to three layers of granulosa cells (Sec-2/3) is not altered. (*D*) The decreased number of ovulated oocytes is caused by impaired ovulation and not by insufficient follicular growth. The number of Graffian follicles with oocytes before (46 h/PMSG) and the number of luteinized follicles with oocytes after ovulation (14h/HCG) was determined in 3-wk-old TAp73$^{+/+}$ and TAp73$^{-/-}$ female mice. The results shown are the mean number of Graffian follicles/mouse ± SE for $n = 5$ mice per group. (**) $P < 0.001$ (Student's *t*-test).

ovulated oocytes in TAp73$^{-/-}$ mice is likely due to the retention of some germ cells within the ovary.

We next investigated whether oocyte quality contributed to TAp73$^{-/-}$ female sterility. Germinal vesicle oo-

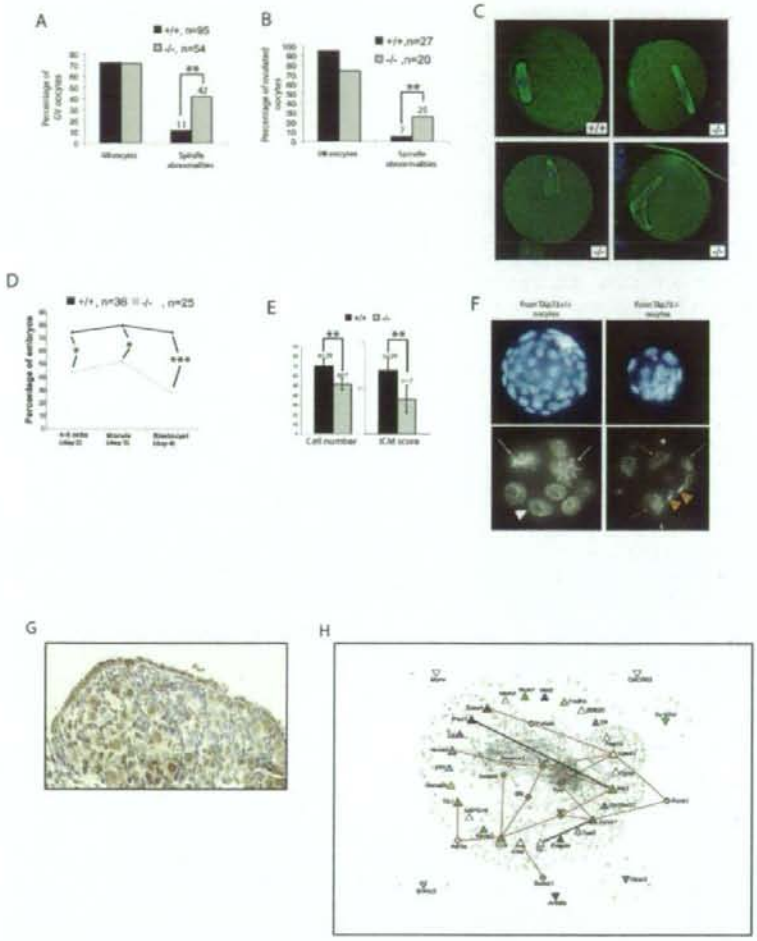

Figure 3. TAp73 deficiency effects on oocyte quality. (*A*,*B*) Quantitation of spindle abnormalities in TAp73$^{+/+}$ and TAp73$^{-/-}$ oocytes matured in vitro (*A*) or in vivo (*B*). While no difference was observed in ability to proceed through the meiosis and arrest in metaphase II (MII), higher numbers of spindle abnormalities were detected in TAp73 oocytes. (**) $P < 0.001$ (Student's *t*-test). (*C*) Representative examples of *B*. Magnification, 40 × 10. (*D*) The IVF procedure showed that no difference exists in the fertilization rate caused by TAp73 deficiency, but progression of zygotes through preimplantation development is abnormal. The percentage of TAp73$^{-/-}$ oocytes that upon fertilization reached the four- to eight-cell, morula, and blastocyst stages at appropriate developmental days is greatly diminished. (*) $P < 0.01$; (***) $P < 0.0001$. Statistical analyses were done using an $X2$ test. (*E*) Poor quality of IVF-derived blastocysts obtained from TAp73$^{-/-}$ oocytes as assessed by total cell number (*left*) and inner cell mass (ICM) score (*right*). (**) $P < 0.001$ (Student's *t*-test). (*F*) DAPI staining of blastocysts (*top*, magnification, 20 × 10) and eight-cell stage-arrested embryos (*bottom*, magnification, 40 × 10) of *B*. (White arrows) Mitotic cells; (white arrowhead) normal nucleus; (red arrows) multinuclear cells; (red arrowheads) sperm heads. (*G*) TAp73 expression in a post-natal day 4 TAp73$^{+/+}$ ovary as detected by immunohistochemical staining with H79 antibody. (*H*) Network visualization of genes that were up-regulated in TAp73$^{+/+}$ and TAp73$^{-/-}$ neonatal ovaries. Node color represents GO (The Gene Ontology) function, as shown in the legend. Node shape represents different targets: Triangles pointed up are targets up-regulated in TAp73$^{-/-}$ ovary; triangles pointing down are targets up-regulated in TAp73$^{+/+}$ ovary. Diamonds and triangles outlined in red represent critical proteins within the network. Thicker lines indicate direct interactions among targets. Red lines represent critical interactions within the network. All other lines represent secondary interacting proteins.

cytes as well as ovulated oocytes from 3- to 4-wk-old TAp73$^{+/+}$ and TAp73$^{-/-}$ mice were induced to mature in vitro. In both cases, oocytes of both genotypes showed the same rate of arrest in metaphase II (Fig. 3A,B, left). However, TAp73$^{-/-}$ oocytes exhibited a striking increase in spindle abnormalities (Fig. 3A,B, right), which included multipolar spindles, spindle relaxation, and spindle scattering accompanied by varying degrees of misalignment (Fig. 3C). We next compared the developmental competence of ovulated TAp73$^{+/+}$ and TAp73$^{-/-}$ oocytes by assessing their ability to undergo in vitro fertilization (IVF) and preimplantation development in vitro. While the fertilization rate was the same, only 28% of zygotes originating from TAp73$^{-/-}$ oocytes became blastocysts, compared with 75% of zygotes originating from TAp73$^{+/+}$ oocytes (Fig. 3D). The majority of embryos obtained from TAp73$^{-/-}$ oocytes arrested during early cleavage, resulting in embryos with multinucleated blastomeres, and blastocysts of inferior quality with an abnormal cell number (Fig. 3E,F). Thus, *Trp73* is a maternal-lethal effect gene, because a lack of TAp73 in developing oocytes leads to a failure of preimplantation embryonic development.

Poor oocyte quality leading to abnormal embryonic development is also associated with maternal aging, and is one of the most important prognostic factors of human infertility. Because oocytes from young TAp73$^{-/-}$ mice displayed a similar spectrum of spindle abnormalities to that observed in oocytes from aged wild-type mice (Tarin et al. 2001), we evaluated TAp73 expression in the ovaries of 8- and 55-wk-old wild-type mice. We found that natural aging abolishes TAp73 expression in oocytes (Supplemental Fig. S4B,C). This observation suggests that loss of TAp73 may be responsible for the compromised developmental capacity of aged normal oocytes.

To identify TAp73 transcriptional targets potentially involved in the regulation of developmental competence, we decided to perform a gene microarray analysis of ovarian tissue. We first used immunocytochemistry to determine what stages of oogenesis were most likely to be affected by a lack of TAp73. Growing wild-type oocytes from the primary follicle stage onward displayed only cytoplasmic expression of TAp73, but the oocytes of wild-type primordial follicles often exhibited nuclear staining (Fig. 3G; Supplemental Fig. S4B). Thus, we used neonatal ovaries, which are enriched in oocytes at this developmental stage, as the target tissue for our microarray analysis. Our results showed that the expression of 79 annotated genes in neonatal ovary was altered by at least 1.8-fold by an absence of TAp73. We confirmed for some genes their modulation of expression in TAp73$^{-/-}$ ovaries compared with wild-type ovaries (Supplemental Fig. S5A,B; data not shown). Among these 79 genes, many were involved in the regulation of transcription and translation via control of RNA processing (see Tables 1, 2). We confirmed that most of these genes are potential or already known p53 targets (Supplemental Fig. S5C). To determine functional links among the differentially regulated targets, we mapped them to the I^{2}D protein interaction database (Brown and Jurisica 2007). Extensive analyses identified several proteins that interacted strongly with TAp73, and also showed that all of these proteins were at points of network disconnect, which suggests that they are essential for signaling within this network (Fig. 3H). Indeed, several of these genes (as example: *PEG10* and *Ctr9*) have been disrupted in animal models with resulting embryonic lethality or infertility (Ono et al. 2006; Akanuma et al. 2007). Taken together, these data suggest that these target genes may normally be regulated by TAp73 or are physical interactors of TAp73, as, for example, in the case of PIAS1 that regulates cell cycle checkpoint progression by sumoylation of TAp73 (Munarriz et al. 2004), and thus their dysregulation may contribute to preimplantation lethality in the absence of TAp73.

TAp73 is necessary for hippocampal development but not for neural cell maintenance

Previous analyses of *Trp73*$^{-/-}$ mice have demonstrated that p73 is critical for the development and maintenance of the nervous system (Yang et al. 2000). Indeed, *Trp73*$^{-/-}$ mice exhibit hippocampal dysgenesis with a gradual but persistent postnatal loss of neurons with greatly enlarged ventricles (hydrocephalus) and greatly reduced cortical tissue (Yang et al. 2000; Pozniak et al. 2002). To investigate whether either of these phenotypes might be due to the loss of TAp73 isoforms, we carried out coronal sectioning of the brains of 10-wk-old wild-type and TAp73$^{-/-}$ mice. Nissl staining of the forebrain revealed that TAp73$^{-/-}$ brains were similar to their wild-type counterparts with regard to the size of the lateral ventricles and the thickness of the cortex (Fig. 4A,B) but that hippocampal anatomy was abnormal. In particular, the lower blade of the dentate gyrus was either completely missing or greatly truncated, depending on the level of the section (Fig. 4C–F). This hippocampal dysgenesis was strikingly similar to that seen in *Trp73*$^{-/-}$ mice at postnatal day 14, before the occurrence of the ventricular enlargement and loss of neural tissue that further perturb hippocampal morphology in adult *Trp73*$^{-/-}$ mice. The similarity between TAp73$^{-/-}$ mice and p73$^{-/-}$ mice on this particular phenotype suggests that it is due to TAp73 loss and not to ΔNp73 loss. Thus, our data support previous work (Pozniak et al. 2000, 2002; Walsh et al. 2004) showing that TAp73 is essential for normal hippocampal development, while ΔNp73 seems to prevent neural tissue loss and ventricular enlargement in adult life.

TAp73$^{-/-}$ mice are tumor-prone and sensitive to carcinogens

While infertility and neural abnormalities detected in the TAp73$^{-/-}$ mice were not identical but reminiscent of those described for Trp73$^{-/-}$ mice (Yang et al. 2000), other aspects of the phenotype were markedly different. Indeed, although the life span of TAp73$^{-/-}$ mice was significantly shorter than that of wild-type mice (Fig. 5A), it

Table 1. *Target genes up-regulated in TAp73$^{-/-}$ ovary compared with wild-type ovary*

Gene ID	Fold change	Gene symbol	Gene title
1417761_at	19.4	Apoa4	Apolipoprotein A-IV
1455201_x_at	4.9	Apoa1	Apolipoprotein A-I
1458915_at	3.4	C77949	Expressed sequence C77949
1457705_at	3.4	5330421C15Rik	RIKEN cDNA 5330421C15 gene
1439304_at	3.3	B230216N24Rik	RIKEN cDNA B230216N24 gene
1427550_at	3.2	Peg10	Paternally expressed 10
1453660_at	3.0	5430420F09Rik	RIKEN cDNA 5430420F09 gene
1439594_at	2.9	D130062J10Rik	RIKEN cDNA D130062J10 gene
1420164_at	2.9	D7E rtd183e	DNA segment, Chromosome 7, ERATO Doi 183, expressed
1433266_at	2.9	2810416A17Rik	RIKEN cDNA 2810416A17 gene
1445881_at	2.8	2310035P21Rik	RIKEN cDNA 2310035P21 gene
1442240_at	2.7	Ctr9	Ctr9, Paf1/RNA polymerase II complex component
1433051_at	2.6	2610011I18Rik	RIKEN cDNA 2610011I18 gene
1431402_at	2.5	Kirrel3	Kin of IRRE like 3 (*Drosophila*)
1446258_at	2.5	9530067D14Rik	RIKEN cDNA 9530067D14 gene
1430575_a_at	2.4	Tpp2	Tripeptidyl peptidase II
1447051_at	2.4	Rnf43	Ring finger protein 43
1453753_at	2.3	Dtl	denticleless homolog (*Drosophila*)
1458097_at	2.3	Cobll1	Cobl-like 1
1453977_at	2.3	Exoc4	Exocyst complex component 4
1432665_at	2.3	2210416J07Rik	RIKEN cDNA 2210416J07 gene
1453361_at	2.2	Hells	Helicase, lymphoid-specific
1439128_at	2.2	Zbtb20	Zinc finger and BTB domain containing 20
1449573_at	2.2	Alpk3	α-Kinase 3
1429870_at	2.1	Tnik	TRAF2 and NCK-interacting kinase
1446827_at	2.1	Ncoa2	Nuclear receptor coactivator 2
1442732_at	2.1	Hadhb	Hydroxyacyl-Coenzyme A dehydrogenase β subunit
1439319_at	2.1	Elf1	E74-like factor 1
1458136_at	2.1	Msi2	Musashi homolog 2 (*Drosophila*)
1438078_at	2.1	Dgke	Diacylglycerol kinase, ε
1451580_a_at	2.1	Ttr	Transthyretin
1456407_a_at	2.1	LOC100046241, Tlk1	tousled-like kinase 1, similar to tousled-like kinase 1
1453448_at	2.1	2310067E 19Rik	RIKEN cDNA 2310067E 19 gene
1431525_at	2.1	9130002K18Rik	RIKEN cDNA 9130002K18 gene
1460233_at	2.1	Guca2b	Guanylate cyclase activator 2b (retina)
1430000_at	2.1	B230117O15Rik	RIKEN cDNA B230117O15 gene
1439095_at	2.1	Sfrs11	Splicing factor, arginine/serine-rich 11
1458737_at	2.0	C77097	Expressed sequence C77097
1458724_at	2.0	E 230008O15Rik	RIKEN cDNA E 230008O15 gene
1427797_s_at	2.0	Ctse	Cathepsin E
1458807_at	2.0	Epb4.1	Erythrocyte protein band 4.1
1455040_s_at	2.0	1110062M06Rik	RIKEN cDNA 1110062M06 gene
1432713_at	2.0	6430709C05Rik	RIKEN cDNA 6430709C05 gene
1446265_at	2.0	Dnm3	Dynamin 3
1446448_at	1.9	Pias1	Protein inhibitor of activated STAT 1
1454299_at	1.9	4833422B07Rik	RIKEN cDNA 4833422B07 gene
1443384_at	1.9	Ptk2	PTK2 protein tyrosine kinase 2
1438842_at	1.9	LOC100039384, LOC	Mitochondrial carrier homolog 2 (*Caenorhabditis elegans*)
1431372_at	1.9	Srpk2	Serine/arginine-rich protein specific kinase 2
1451456_at	1.9	6430706D22Rik	RIKEN cDNA 6430706D22 gene
1443121_at	1.9	Calcoco1	Calcium binding and coiled-coil domain 1
1455987_at	1.9	Sec61a1	Sec61 α1 subunit (*Saccharomyces cerevisiae*)
1426028_a_at	1.9	Cit	Citron
1456166_at	1.8	Ehd2	EH-domain containing 2
1431761_at	1.8	Entpd4	Ectonucleoside triphosphate diphosphohydrolase 4
1454524_at	1.8	2310075M01Rik	RIKEN cDNA 2310075M01 gene
1439363_at	1.8	1200014J11Rik	RIKEN cDNA 1200014J11 gene
1444684_at	1.8	8030475D13Rik	RIKEN cDNA 8030475D13 gene
1439213_at	1.8	Ston1	Stonin 1
1451577_at	1.8	Zbtb20	Zinc finger and BTB domain containing 20

Table 2. *Target genes down-regulated in TAp73$^{-/-}$ ovary compared with wild-type ovary*

Gene ID	Fold change	Gene symbol	Gene title
1436386_x_at	−2.8	OTTMUS G 00000010671	Predicted gene, OTTMUS G 00000010671
1446469_at	−2.6	E G 328,231	Predicted gene, E G 328,231
1419119_at	−2.1	Hcst	Hematopoietic cell signal transducer
1438757_at	−2.1	LOC 100,043,772	Similar to crooked legs C G 14938-PB
1420792_at	−2.1	4930433N12Rik	RIKEN cDNA 4930433N12 gene
1428077_at	−2.0	Tmem163	Transmembrane protein 163
1428985_at	−2.0	Ints12	Integrator complex subunit 12
1429366_at	−1.9	Lrrc34	Leucine-rich repeat containing 34
1421099_at	−1.9	Bhlhb3	Basic helix–loop–helix domain containing, class B3
1452972_at	−1.9	Ttc32	Tetratricopeptide repeat domain 32
1442176_at	−1.9	Arid5b	AT-rich interactive domain 5B (Mrf1 like)
1429118_a_at	−1.9	Zh2c2	Zinc finger, H2C2 domain containing
1421333_a_at	−1.9	Mynn	Myoneurin
1419372_at	−1.8	Gosr2	Golgi SNAP receptor complex member 2
1457127_at	−1.8	Defb42	Defensin β 42
1450895_a_at	−1.8	1810020G 14Rik	RIKEN cDNA 1810020G 14 gene

still exceeded that of *Trp73*$^{-/-}$ mice (Yang et al. 2000). Furthermore, whereas untreated *Trp73*$^{-/-}$ mice do not develop tumors, 30% of TAp73$^{+/-}$ and 73% of TAp73$^{-/-}$ mice of a mixed genetic background spontaneously developed malignancies (Fig. 5B,C). Lung adenocarcinoma was the most frequent cancer that developed in TAp73$^{-/-}$ mice, being observed in 32% of all TAp73$^{-/-}$ mice analyzed and representing 44% of all tumors excised from TAp73$^{-/-}$ mice. In the lung of the TAp73$^{-/-}$ knockout, no changes in either ΔNp73 mRNA or protein compared with wild-type were observed (see above). Importantly, no correlation was found between tumor onset and p53, p63, or ΔNp73 protein expression in any tumor analyzed (data not shown), suggesting that the appearance of tumors in TAp73$^{+/-}$ and TAp73$^{-/-}$ mice was specifically due to TAp73 deletion rather than to ΔNp73, p63, or p53 deregulation. Consistent with a previous report (Roman-Gomez et al. 2006), loss-of-heterozygosity (LOH) of p73 had occurred in 66% of tumors developing in TAp73$^{+/-}$ mice (Fig. 5D).

To confirm the tumor-prone phenotype of TAp73$^{-/-}$ mice, we induced carcinogenesis by intraperitoneal injection of DMBA into TAp73$^{+/+}$ and TAp73$^{-/-}$ female littermates. The mean latency time for tumor development in TAp73$^{-/-}$ mice was 18.7 ± 7.1 wk, significantly shorter than the 32 ± 3.4-wk mean latency observed in DMBA-treated TAp73$^{+/+}$ mice (Fig. 5E). However, there was no difference between DMBA-treated TAp73$^{+/+}$ and TAp73$^{-/-}$ mice in sites of tumor development, which included the colon, intestine, liver, and stomach (data not shown). These results indicate that TAp73 isoforms mediate the tumor-suppressive function of *Trp73*, and that loss of TAp73 alone is sufficient to promote oncogenic transformation.

Taking into account the observation that TAp73$^{-/-}$ mice develop predominantly lung adenocarcinoma, we decided to investigate the expression of p73 isoforms in human lung cancer. Examination of the expression of TAp73 and ΔNp73 in matched normal and tumoral lung tissue samples from 18 lung cancer patients revealed that most tumoral lung samples exhibited a down-regulation of TAp73 and an up-regulation of ΔNp73, with a consequent decrease in the TAp73/ΔNp73 ratio (Supplemental Fig. S6). Notably, in the two samples (patients 133 and 177) in which TAp73 expression was up-regulated, greater amounts of ΔNp73 were also expressed. These results are consistent with the postulated inactivation of p53 in human lung cancer (Haruki et al. 2001).

TAp73 participates in maintenance of genomic stability

Since we observed an increased incidence of spontaneous tumors and also an abnormal spindle formation in the oocytes of TAp73$^{-/-}$ mice, we next investigated the possible impact of TAp73 deficiency on the maintenance of genomic stability. Accurate chromosome segregation during meiosis and mitosis is critical to the preservation of euploidy in eukaryotic cells (Yuen et al. 2005), and errors in the molecular mechanisms regulating segregation result in aneuploidy (Hassold and Hunt 2001; Thomas et al. 2001). We analyzed the ability of TAp73-deficient cells to undergo mitotic arrest and observed that TAp73$^{-/-}$ MEFs showed a significant decrease in nocodozole-induced mitotic arrest. Indeed, at 25 h post-nocodozole, the percentages of cells in G1 and >G2/M were increased in TAp73$^{-/-}$ MEFs compared with TAp73$^{+/+}$ MEFs (Fig. 6A; Supplemental Fig. S7A). Immunoblotting of mitotic phase marker proteins such as cyclin B1 and securin revealed that mitotic "slippage" had occurred in TAp73$^{-/-}$ MEFs (data not shown). Premature mitotic exit in TAp73$^{-/-}$ MEFs was confirmed by immunostaining to detect phospho-histone H3-positive cells (Fig. 6B) and by counting mitotic figures (Fig. 6C, right). Thus, in the presence of nocodazole, TAp73 deficiency results in the abnormal mitotic progression of cells that otherwise would not be permitted to pass into the G1 phase. We observed a similar premature mitotic exit in p73$^{-/-}$ MEF cells treated with nocodazole, strongly suggesting that TAp73 isoforms are the functional isoforms

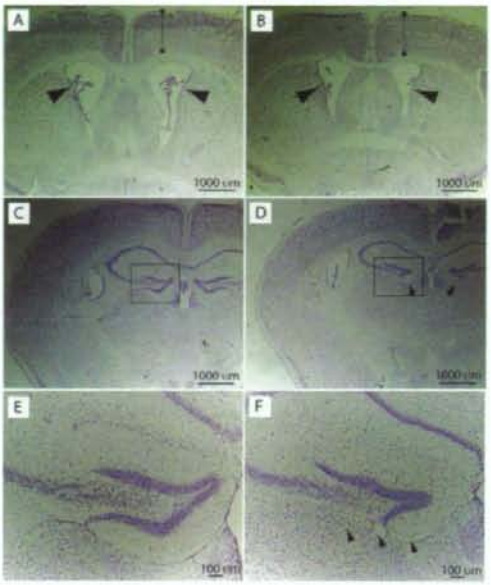

Figure 4. TAp73 is essential for normal hippocampal development. Representative pictures from multiple experiments using seven TAp73$^{+/+}$ and seven TAp73$^{-/-}$ mice of coronal forebrain sections of 4-mo-old TAp73$^{+/+}$ (*A,C,E*) and TAp73$^{-/-}$ (*B,D,F*) C57B6 background mice stained with cresyl violet. (*A,B*) Nissl-stained coronal sections of forebrain at the level of the anterior commissure. Arrows indicate the lateral ventricles. Cortical thickness (brackets) was similar in TAp73$^{+/+}$ and TAp73$^{-/-}$ brains. (*C–F*) Nissl-stained coronal sections of the forebrain at the level of the rostral hippocampus. The area denoted by the boxes in *C* and *D* is shown at higher magnification in *E* and *F*, respectively. Arrows in *D* and *F* denote the site of the lower blade of the dentate gyrus, which is missing in the TAp73$^{-/-}$ brain.

in mitotic regulation rather than ΔNp73 isoforms (Supplemental Fig. S7B,C).

After 25 h of nocodazole treatment, an 8N population of polyploid cells appeared frequently among TAp73$^{-/-}$ MEFs when compared with TAp73$^{+/+}$ MEFs (Fig. 6A). Indeed, ~14% of TAp73$^{-/-}$ MEFs showed aneuploidy compared with 5% of cells in TAp73$^{+/+}$ MEF cultures. The percentage of multinuclear cells was also increased in TAp73$^{-/-}$ MEFs treated with taxol or nocodozole (Fig. 6C, left). When H1299 cells were engineered to overexpress the TAp73β isoform, they were protected from taxol-induced formation of multinuclear cells (Fig. 6D). In contrast, overexpression of ΔNp73α or ΔNp73β in *Trp73*$^{-/-}$ MEFs did not reduce the enhanced formation of multinuclear cells (data not shown).

We next examined lung and thymic cell populations from TAp73$^{-/-}$, *Trp53*$^{-/-}$, and wild-type mice that were treated or not with nocodazole for 12 h. TAp73$^{-/-}$ lung fibroblasts showed a higher frequency of >G2/M cells, demonstrating a loss of euploidy, which are likely aneuploid, than did *Trp53*$^{-/-}$ or wild-type lung fibroblasts, whereas no differences were observed among TAp73$^{-/-}$, *Trp53*$^{-/-}$, and wild-type thymic cells (Fig. 6E,F). Thus, the effect of TAp73 on aneuploidy appears to be tissue-specific, perhaps explaining why TAp73$^{-/-}$ mice preferentially develop lung adenocarcinomas. Our results indicate that, at least in lung tissue, TAp73 loss is associated with decreased genomic stability.

To confirm more directly that TAp73 deficiency is associated with an altered DNA content, we karyotyped TAp73$^{-/-}$ and TAp73$^{+/+}$ 3T3 cells and observed that the mutant cultures contained a significantly higher percentage of cells with an abnormal karyotype compared with wild-type controls (Fig. 6G). The affected cells showed a loss or gain of a single chromosome, indicating aneuploidy. These data further support a role for TAp73 in maintaining genomic stability.

Discussion

As mentioned above, mouse models featuring deletion of all p73 isoforms (Yang et al. 2000), or p73 deletion in combination with *Trp53* deficiency (Flores et al. 2005; Perez-Losada et al. 2005), or overexpression of specific p73 isoforms (Huttinger-Kirchhof et al. 2006), have all been helpful in dissecting the role of *Trp73* in various biological processes. However, these mouse models cannot distinguish between the effects of the TAp73 and ΔNp73 isoforms, so that the relative importance of these isoforms in specific biological processes remains unclear or even conflicting. In our study, we generated and analyzed the effects of a selective deficiency of TAp73 isoforms. Our comparison of the phenotypes of *Trp73*$^{-/-}$ and TAp73$^{-/-}$ mice has clearly identified several functions that require TAp73 as opposed to ΔNp73. However, single isoform deletion models, the complete deletion of all isoforms, and even partial deletions and hypomorphic models will all be needed to completely understand the complex functional network mediated by p53 family members.

Both *Trp73*$^{-/-}$ and TAp73$^{-/-}$ mice are infertile, but the root causes of this infertility differ. *Trp73*$^{-/-}$ mice have sensory defects that prevent them from mating normally (Yang et al. 2000). In contrast, TAp73$^{-/-}$ female mice mate normally but have oocytes of reduced developmental competence that result in impaired early embryogenesis. The increased frequency of spindle defects in TAp73$^{-/-}$ ovulated oocytes may also contribute to the sterility of TAp73$^{-/-}$ females, in line with the strong correlation of this parameter with human infertility (Baird et al. 2005). Importantly, our work has identified *Trp73* as one of a handful of genes whose mutation generates a maternal lethal effect phenotype. Genes belonging to this group are required for the transition from maternal to embryonic control over embryogenesis. Accordingly, the spectrum of cellular defects observed in embryos originating from TAp73$^{-/-}$ oocytes is remarkably similar to the range of embryonic defects observed in infertile patients undergoing IVF, particularly older patients (Har-

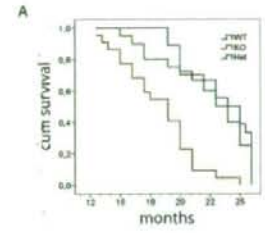

B

Tumor type	Genotype +/+ (n=18)	+/- (n=20)	-/- (n=22)
Thymic lymphoma	0/18 (0%)	1/20 (5%)	3/22 (14%)
Lymphoma	1/18 (6%)	2/20 (10%)*	4/22 (18%)*
Lung adenocarcinoma	0/18 (0%)	1/20 (5%)	7/22 (32%)
Colon carcinoma-in-situ	0/18 (0%)	1/20 (5%)	2/22 (9%)
Hemangiosarcoma	0/18 (0%)	1/20 (5%)	0/22 (0%)
Total tumor number (% of total)	1/18 (6%)	6/20 (30%)	16/22 (73%)

* all these mice have infiltrating lymphoma in more than one organ

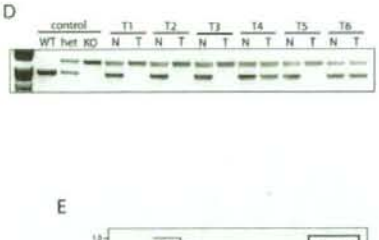

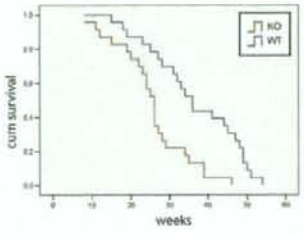

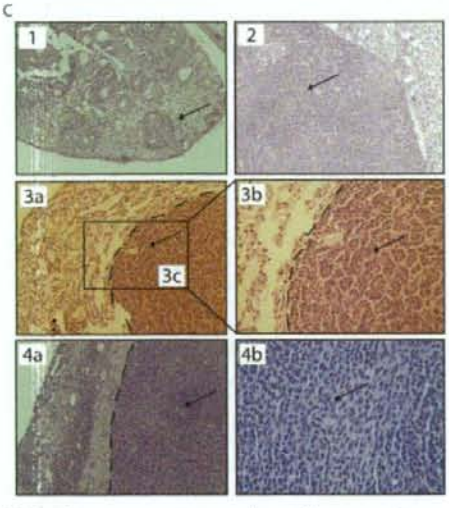

Figure 5. TAp73$^{-/-}$ mice are tumor-prone and sensitive to carcinogens. (*A*) Kaplan-Meyer survival curves of TAp73$^{+/+}$ (n = 18), TAp73$^{+/-}$ (n = 20), and TAp73$^{-/-}$ (n = 22) mice. $P < 0.001$ (Logrank test). (*B*) Spontaneous tumor spectrum in TAp73$^{+/+}$, TAp73$^{+/-}$, and TAp73$^{-/-}$ mice. Spontaneous tumor development in TAp73$^{-/-}$ mice is significative with a P-value of $P < 0.005$ ($X2$ Test). (*C*, arrows) H&E-stained tumors in tissues of TAp73$^{-/-}$ mice. (1) Colon carcinoma in situ, 10× magnification. (2) Invasive lymphoma in ovary, 10× magnification. (3a–3c) Lung adenocarcinoma, 10× magnification, with 3b being a higher magnification of 3c, 20× magnification. (4a–4b) Invasive lymphoma in uterus, 10× magnification, with 4b being a higher magnification of 4a, 40× magnification. Dotted lines denote the border between healthy and tumoral tissue. (*D*) Representative LOH analysis of six TAp73$^{+/-}$ tumor-bearing mice (T1-6); (T) tumor; (N) normal tissue. (*E*) Kaplan-Meyer survival curves of DMBA-treated TAp73$^{+/+}$ (n = 23) and TAp73$^{-/-}$ (n = 23) mice in weeks after treatment. $P < 0.005$ (Logrank test).

darson et al. 2001; Hardy et al. 2001). These data are also consistent with the down-regulation of p73 transcripts that occurs in the oocytes of older patients (Steuerwald et al. 2007). The p53-family members are pivotal in the control of aging, as shown for p63 (Keyes et al. 2005; Suh et al. 2006), p53 mutant (Tyner et al. 2002), or deficient mice (Ohkusu-Tsukada et al. 1999). Regarding our results, it would be of interest that TAp73 down-regula-

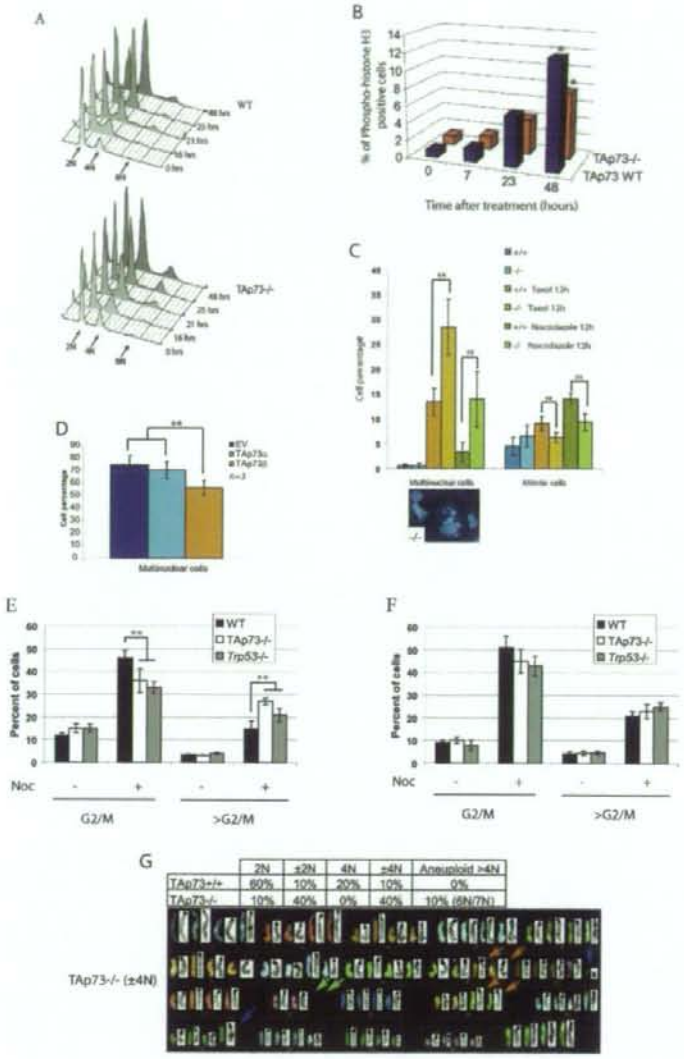

	2N	±2N	4N	±4N	Aneuploid >4N
TAp73+/+	60%	10%	20%	10%	0%
TAp73-/-	10%	40%	0%	40%	10% (6N/7N)

Figure 6. Defective maintenance of genomic stability in the absence of TAp73. (*A*) Cell cycle analysis by flow cytometry of TAp73$^{+/+}$ (*top*) and TAp73$^{-/-}$ (*bottom*) MEFs treated with nocodazole for the indicated number of hours. The graph was created using FlowJo 7.2.2 software. (*B*) Percentage of phospho-histone H3^{+} cells in cultures of TAp73$^{+/+}$ (TAp73 wild type) and TAp73$^{-/-}$ MEFs treated with nocodazole for indicated times. (*) $P < 0.01$ (Student's *t*-test). (*C*) Percentages of multinuclear (*left*) and mitotic (*right*) cells in TAp73$^{+/+}$ and TAp73$^{-/-}$ MEFs treated with taxol or nocodazole as indicated. (*Bottom*) DAPI-stained multinuclear TAp73$^{-/-}$ MEFs, 40× magnification. The data shown represent the mean ± SE of three different experiments. (**) $P < 0.001$ (Student's *t*-test). (*D*) Percentage of multinuclear cells in H1299 cultures overexpressing empty vector (EV) or vector containing the indicated TAp73 isoforms and treated with taxol for 24 h. (**) $P < 0.001$ (Student's *t*-test). (*E*,*F*) Percentages of cells in G2/M phase or in >G2/M phase (aneuploid cells). Cells were extracted from the lung (*E*) or thymus (*F*) of wild-type, TAp73$^{-/-}$, and *Trp53*$^{-/-}$ mice and treated for 12 h with nocodazole. The results shown are the mean percentage of cells ± SE of three independent trials. (**) $P < 0.001$ (Student's *t*-test). (*G*) Increased aneuploidy. (*Top*) Percentages of cells in TAp73$^{+/+}$ and TAp73$^{-/-}$ 3T3 cultures showing diploid (2N), near-diploid (±2N), tetraploid (4N), near-tetraploid (±4N), and aneuploid (>4N) DNA content. (*Bottom*) Representative karyotype of a ±4N TAp73$^{-/-}$ 3T3 cell.

tion, due to aging or loss-of-function mutations, may be a potential prognostic factor in cases of human female infertility.

In addition to infertility, TAp73$^{-/-}$ mice exhibited a mild defect in brain morphology. Hippocampal dysgenesis was observed in TAp73$^{-/-}$ mice, but there were no signs of neural tissue loss or ventricular enlargement as occur in *Trp73*$^{-/-}$ mice. Based on our studies and those of *Trp73*-deficient mice, we suggest that a lack of the ΔNp73 isoform rather than TAp73 is responsible for neural tissue loss and ventricular enlargement in the brain, whereas hippocampal dysgenesis with loss or severe truncation of the dentate gyrus is specifically linked to TAp73 deficiency. The generation and characterization of a mouse with a selective deficiency of ΔNp73 is needed to completely resolve this question.

Our study is the first clear demonstration that TAp73 isoforms possess the tumor-suppressive ability of *Trp73*, and thus resolves previous conflicting results (McKeon and Melino 2007). It has been proposed previously that a loss of p73 function might lead to tumorigenesis (Flores et al. 2002, 2005), and that TAp73 down-regulation may

be coupled with ΔNp73 up-regulation in some tumors (Zaika et al. 2002). We found that mice with a selective deficiency of TAp73 develop spontaneous tumors, particularly lung adenocarcinomas, and are more sensitive to chemical carcinogens. The development of spontaneous tumors in TAp73$^{-/-}$ mice but not in *Trp73*$^{-/-}$ mice illustrates the complex relationship between *Trp53* family members and cancer.

Intriguingly, the types of tumors detected in TAp73$^{-/-}$ mice, as well as those detected in *Trp63*$^{+/-}$ and *Trp73*$^{+/-}$ mice, are quite different from the range of malignancies displayed by *Trp53*$^{-/-}$ mice (even taking strain differences into account) (Flores et al. 2002, 2005). Furthermore, although p63 and p73 do not contribute to p53-mediated suppression of murine lymphomagenesis in vivo (Perez-Losada et al. 2005), allelic loss and genetic instability of *Trp73* have been linked to non-Hodgkin's lymphomas (Martinez-Delgado et al. 2002). These potentially conflicting data and the diversity in tumor spectra in these various models are likely due to the intricate pattern of expression of multiple p53, p63, and p73 isoforms. Human cancer cells can express peculiarly spliced isoforms of p73, such as Δ2p73 and Δ2,3p73 (Pützer et al. 2003; Concin et al. 2004), that involve selective deletions of *Trp73* exons 2 and 3. These cancer cells show both elimination of the TAp73 isoform and up-regulation of a ΔNp73 variant, mimicking our TAp73$^{-/-}$ mice, and developing a strikingly similar phenotype. Our mouse model therefore highlights the complex interregulation of TAp73 and ΔNp73 isoforms and closely reflects the aberrant pattern of p73 expression in many human cancers.

More and more evidence implicates p53 and its family members in the prevention of genomic instability, aneuploidy, and cancer, although the details of the molecular links remain unclear (Duensing and Duensing 2005). Inactivation of p53 family members may lead to a chromosomal instability phenotype that is a hallmark of cancers in which specific mitotic proteins are dysregulated (Carter et al. 2006; for review, see Tomasini et al. 2008). A recent report has shown that the combined loss of *Trp73* and *Trp53* induces severe genomic instability and a rapid increase in polyploidy and aneuploidy that markedly exceeds that induced by loss of *Trp53* alone (Talos et al. 2007). In addition, *Trp73* seems necessary for the death of cells undergoing abnormal mitosis (Niikura et al. 2007). These results are in line with the abnormal survival described in our TAp73$^{-/-}$ cells with elevated (more than 4N) DNA content. The persistence of these genetically unstable cells could then set the stage for tumorigenesis.

Our data demonstrate that TAp73 isoforms are bona fide tumor suppressors, contributing to the growing body of evidence linking genomic instability and aneuploidy with tumorigenesis (Pérez de Castro et al. 2007; Weaver and Cleveland 2007). Specifically, our findings point to a critical emerging role for the TAp73 isoform in the maintenance of genomic stability that prevents both tumor formation and infertility. Indeed, like p53 (Hu et al. 2007) and p63 (Suh et al. 2006), the entire p53 family seems to act as "the guardian of the female germline."

Materials and methods

Generation of TAp73$^{-/-}$ mice and LOH analysis

Mutant mice deficient for *Trp73* exons 2 and 3, which are specific for the TAp73 isoforms, were generated by conventional gene targeting procedures in Sv129Ola embryonic stem cells. Blastocysts were transferred to pseudopregnant C57BL/6J female mice. TAp73 wild-type (wild type, +/+; TAp73$^{+/+}$), heterozygous (+/−; TAp73$^{+/-}$), and homozygous (−/−; TAp73$^{-/-}$) littermate mice (Sv129Ola × C57BL/6J) were created by intercrossing TAp73$^{+/-}$ mice. Offspring were genotyped by PCR analysis using specific primer pairs to detect the wild-type *Trp73* and *Trp73*$^{\Delta TA}$ alleles. Sense and antisense primers for the wild-type *Trp73* allele were 5′-CTGGTCCAGGAGGTGAGACTGAG GC-3′ and 5′-CTGGCCCTCTCAGCTTGTGCCACTTC-3′, respectively. Sense and antisense primers for the gene-targeted *Trp73*$^{\Delta TA}$ allele were 5′-GTGGGGGTGGGATTAGATAAAT GCCTG-3′ and 5′-CTGGCCCTCTCAGCTTGTGCCACTTC-3′, respectively. Predicted PCR product sizes were 1.0 kb and 1.2 kb for the wild-type *Trp73* and *Trp73*$^{\Delta TA}$ alleles, respectively. F4 mixed background mice were used for all experiments except the analysis of the Mendelian ratio, for which we also used animals of the fifth-generation backcross in a C57B6 background. All animals were treated in accordance with the NIH Guide for Care and Use of Laboratory Animals as approved by the Ontario Cancer Institute Animal Care Committee (Toronto, ON, Canada). LOH analysis was performed using genotyping primers and PCR amplification of *Trp73* exons 2 and 3 in genomic DNA from tumor and normal (tail) tissues of tumor-bearing TAp73$^{+/-}$ mice.

Analyses of spontaneous and induced tumors

Life span and spontaneous tumor incidence were determined in untreated TAp73$^{+/+}$ and TAp73$^{-/-}$ mice. Mice with visible tumors and moribund mice showing weight loss or difficulties in moving were sacrificed upon detection. The remaining surviving mice were sacrificed at 26 mo of age. For induced tumorigenesis, TAp73$^{+/+}$ and TAp73$^{-/-}$ mice (23 mice/group) were injected i.p. with 1 mg/kg dimethylbenz[a]anthracene (DMBA; Sigma-Aldrich) starting at 63 d post-partum and continuing once a week for 6 wk. This dose was sufficient to induce 100% tumor incidence in controls. Tumors and tissues of control and mutant mice were collected and processed for histopathology and RNA/DNA isolation by standard procedures.

Oocyte collection, in vitro maturation, and in vitro fertilization

Female mice (3–7 wk old) were superovulated, and mature oocytes were collected as previously described (Perez et al. 2005). For in vitro maturation, germinal vesicle stage oocytes from 3-wk-old females were induced to undergo spontaneous in vitro maturation (Yao et al. 2004), and in vitro fertilization was carried out as described previously (Acton et al. 2004). Embryonic developmental competence was assessed daily. On day 4, embryos were fixed and cell number, cell death, and mitotic rates were determined as described previously (Jurisicova et al. 1998). Statistics were obtained using the χ^2 or Student's *t*-test.

Microarray studies

Microarray analysis was performed on day 4 ovarian tissue from two sibling pairs of TAp73$^{+/+}$ and TAp73$^{-/-}$ females by the Cen-

ter for Applied Genomics (Hospital for Sick Children, Toronto) using the Affymetrix platform (Mouse MOE 430 2.0) with two cycle amplification steps. Data were preprocessed using RMA-Express 1.0 beta 3 (Bolstad et al. 2003), $\log_2$ transformed, and then analyzed using SAM version 3.0 (Tusher et al. 2001). Using FDR (False Discovery Rate) = 0.603%, we identified 2538 genes that were differentially expressed (1178 up-regulated and 1360 down-regulated in TAp73$^{-/-}$ ovaries). To further diminish false positives, we prioritized the genes by considering only fold change >1.8, which resulted in 16 genes up-regulated and 60 genes down-regulated in wild-type ovaries.

To determine functional links among identified target genes, we mapped them to the Interologous Interaction Database I^{2}D ver. 1.71 (http://ophid.utoronto.ca/i2d). A network was formed containing 531 proteins and 977 interactions on seven targets up-regulated in TAp73$^{+/+}$ ovaries and 26 targets up-regulated in TAp73$^{-/-}$ ovaries. Further visualization and analysis of the resulting protein interaction network were performed using NAViGaTOR ver 2.0 (http://ophid.utoronto.ca/navigator). Shortest path calculations were used to determine critical proteins and interactions. Briefly, the shortest path among all nodes within the network was computed, and the frequency of inclusion of individual proteins and interactions was counted. The most frequent nodes and lines form the critical subgraph within the network. We applied blending to reduce network complexity (NAViGaTOR version 2.0).

Immunohistochemical analysis

For histological analysis of mouse brains, sacrificed animals were perfused with 4% paraformaldehyde, and their brains were cryoprotected, sectioned, and Nissl-stained as described previously (Pozniak et al. 2002). For histological analysis of oocytes, oocyte fixation and immunocytochemistry were performed as described previously (Yao et al. 2004). Samples were viewed on a deconvolution fluorescence microscope. Follicular histomorphology was performed on fixed ovarian tissue obtained from 3-wk-old females (Canning et al. 2003), and immunocytochemistry on ovarian sections was performed as described previously (Matikainen et al. 2001). The antibodies used for analyses of oocytes and/or ovarian sections were rat monoclonal anti-tubulin (YL1/2; Abcam), rabbit polyclonal anti-p73 (H79; Santa Cruz Biotechnologies), and goat anti-p73α (C17; Santa Cruz Biotechnologies). For spindle analyses, secondary antibody was conjugated to Oregon green (Molecular Probes). For ovarian sections, visualization was performed using a biotinylated anti-rabbit antibody detection kit (DAKO).

Cell lines and overexpression experiments

MEFs obtained from embryonic day 13.5 (E13.5) TAp73$^{+/+}$, TAp73$^{-/-}$, and p73$^{-/-}$ embryos, or 3T3 cells, were cultured in Dulbecco's modified Eagle's medium (DMEM) supplemented with 10% FCS without antibiotics. For overexpression experiments, the human lung carcinoma cell line H1299 was plated at 60% density the day before transfections. Transient transfection of plasmids was carried out using the FuGENE reagent (Roche Applied Science) according to the manufacturer's protocol. Control vector pcDNA3-HA was from Clontech. DNA sequences encoding the TAp73α and TAp73β isoforms were all cloned in pcDNA3-HA.

Flow cytometric analyses

TAp73$^{-/-}$ MEFs were seeded at 3×10^5 cells per 100-mm plate. Cultures were then either left untreated or treated with nocodazole (200 ng/mL; Sigma-Aldrich). Immediately (control) or at 16, 21, 25, or 48 h after nocodazole treatment, cells were harvested and fixed for at least 1 h at 4°C in PBS/70% ethanol. Fixed cells were resuspended in PBS containing 100 µg/mL RNase A and 50 µg/mL propidium iodide (Sigma-Aldrich) and immediately analyzed using a FACSCalibur (Becton Dickinson Biosciences). Data were collected and analyzed with CellQuest Pro (BD Biosciences) and FlowJo 7.2.2 Data Analysis Software. Phospho-histone H3 staining was performed using an anti-phospho-histone H3 antibody (#9708; Cell Signaling) according to the manufacturer's protocol. Cell cycle analysis of total cell populations from fresh TAp73$^{+/+}$, TAp73$^{-/-}$, and p53$^{-/-}$ thymus or lung tissues was performed as previously described (Yamamoto et al. 2003).

Cell death analysis was performed by flow cytometry using propidium iodide staining together with AnnexinV-FITC as described previously.

Western blotting

Protein extracts (100 µg) were fractionated by SDS-PAGE and subjected to Western blotting by standard procedures. Western blots were quantified by band densitometry using an Odyssey Infrared Imaging System (LI-COR Biosciences). For immunoprecipitations, protein extracts from MEFs were analyzed according to standard protocols. The antibodies used for Western blot were mouse anti-ΔNp73 (IMG-313; Imgenex), goat anti-p73 (C-20; Santa Cruz), rabbit anti-phospho-p53 ser15 (#9284L; Cell Signaling), and rabbit anti-p53 total (CM5; Vector Laboratories).

Acknowledgments

We gratefully acknowledge H. Okada and R.A. Knight for technical advice and helpful discussions, P. Berthezene for statistical analysis, S.K. Lau for technical help with human real-time PCR analysis, and M.E. Saunders for scientific editing. This work was supported by grants from AIRC, EU (Active-p53, Epistem), FIRB, MIUR, and MinSan to G.M. R.T. was supported by l'Association pour la recherche contre le cancer. R.T, K.T., and A.J. were supported by the Canadian Institutes of Health Research. R.T., K.T., M.W., M.F., A.R., C.C.C., F.K., A.I.-Y., A.W., P.B., and A.J. conducted research for the paper. R.T., G.M., A.J., and T.W.M. wrote the paper. We all discussed the results and read the paper.

References

Acton, B.M., Jurisicova, A., Jurisica, I., and Casper, R.F. 2004. Alterations in mitochondrial membrane potential during preimplantation stages of mouse and human embryo development. *Mol. Hum. Reprod.* **10:** 23–32.

Akanuma, T., Koshida, S., Kawamura, A., Kishimoto, Y., and Takada, S. 2007. Paf1 complex homologues are required for Notch-regulated transcription during somite segmentation. *EMBO Rep.* **8:** 858–863.

Baird, D.T., Collins, J., Egozcue, J., Evers, L.H., Gianaroli, L., Leridon, H., Sunde, A., Templeton, A., Van Steirteghem, A., Cohen, J., et al. 2005. Fertility and ageing. *Hum. Reprod. Update* **11:** 261–276.

Bolstad, B.M., Irizarry, R.A., Astrand, M., and Speed, T.P. 2003. A comparison of normalization methods for high density oligonucleotide array data based on bias and variance. *Bioinformatics* **19:** 185–193.

Bourdon, J.C., Fernandez, K., Murray-Zmijewski, K., Liu, G., Diot, A., Xirodimas, D.P., Saville, M.K., and Lane, D.P. 2005.

p53 isoforms can regulate p53 transcriptional activity. *Genes & Dev.* **19:** 2122–2137.

Brown, K. and Jurisica, I. 2007. Unequal evolutionary conservation of human protein interactions in interologous networks. *Genome Biol.* **8:** R95. doi: 10.1186/gb-2007-8-5-r95.

Canning, J., Takai, Y., and Tilly, J.L. 2003. Evidence for genetic modifiers of ovarian follicular endowment and development from studies of five inbred mouse strains. *Endocrinology* **144:** 9–12.

Carter, S.L., Eklund, A.C., Kohane, I.S., Harris, L.N., and Szallasi, Z. 2006. A signature of chromosomal instability inferred from gene expression profiles predicts clinical outcome in multiple human cancers. *Nat. Genet.* **38:** 1043–1048.

Coates, P.J. 2006. Regulating p73 isoforms in human tumours. *J. Pathol.* **210:** 385–389.

Concin, N., Becker, K., Slade, N., Erster, S., Mueller-Holzner, E., Ulmer, H., Daxenbichler, G., Zeimet, A., Zeillinger, R., Marth, C., et al. 2004. Transdominant ΔTAp73 isoforms are frequently up-regulated in ovarian cancer. Evidence for their role as epigenetic p53 inhibitors in vivo. *Cancer Res.* **64:** 2449–2460.

De Laurenzi, V., Costanzo, A., Barcaroli, D., Terrinoni, A., Falco, M., Annicchiarico-Petruzzelli, M., Levrero, M., and Melino, G. 1998. Two new p73 splice variants, γ and δ, with different transcriptional activity. *J. Exp. Med.* **188:** 1763–1768.

Deyoung, M.P. and Ellisen, L.W. 2007. p63 and p73 in human cancer: Defining the network. *Oncogene* **26:** 5169–5183.

Donehower, L.A., Harvey, M., Slagle, B.L., McArthur, M.J., Montgomery Jr., C.A., Butel, J.S., and Bradley, A. 1992. Mice deficient for p53 are developmentally normal but susceptible to spontaneous tumours. *Nature* **356:** 215–221.

Duensing, A. and Duensing, S. 2005. Guilt by association? p53 and the development of aneuploidy in cancer. *Biochem. Biophys. Res. Commun.* **331:** 694–700.

Erster, S., Palacios, G., Rosenquist, T., Chang, C., and Moll, U.M. 2006. Deregulated expression of ΔNp73α causes early embryonic lethality. *Cell Death Differ.* **13:** 170–173.

Flores, E.R., Tsai, K.Y., Crowley, D., Sengupta, S., Yang, A., McKeon, F., and Jacks, T. 2002. p63 and p73 are required for p53-dependent apoptosis in response to DNA damage. *Nature* **416:** 560–564.

Flores, E.R., Sengupta, S., Miller, J.B., Newman, J.J., Bronson, R., Crowley, D., Yang, A., McKeon, F., and Jacks, T. 2005. Tumor predisposition in mice mutant for p63 and p73: Evidence for broader tumor suppressor functions for the p53 family. *Cancer Cell* **7:** 363–373.

Grob, T.J., Novak, U., Maisse, C., Barcaroli, D., Lüthi, A.U., Pirnia, F., Hügli, B., Graber, H.U., De Laurenzi, V., Fey, M.F., et al. 2001. Human ΔNp73 regulates a dominant negative feedback loop for TAp73 and p53. *Cell Death Differ.* **8:** 1213–1223.

Hardarson, T., Hanson, C., Sjogren, A., and Lundin, K. 2001. Human embryos with unevenly sized blastomeres have lower pregnancy and implantation rates: Indications for aneuploidy and multinucleation. *Hum. Reprod.* **16:** 313–318.

Hardy, K., Spanos, S., Becker, D., Iannelli, P., Winston, R.M., and Stark, J. 2001. From cell death to embryo arrest: Mathematical models of human preimplantation embryo development. *Proc. Natl. Acad. Sci.* **98:** 1655–1660.

Haruki, N., Harano, T., Masuda, A., Kiyono, T., Takahashi, T., Tatematsu, Y., Shimuzu, S., Mitsudomi, T., Konishi, H., Osada, H., et al. 2001. Persistent increase in chromosome instability in lung cancer: Possible indirect involvement of p53 inactivation. *Am. J. Pathol.* **159:** 1345–1352.

Hassold, T. and Hunt, P. 2001. To err (meiotically) is human: The genesis of human aneuploidy. *Nat. Rev. Genet.* **2:** 280–291.

Hu, W., Feng, Z., Teresky, A.K., and Levine, A.J. 2007. p53 regulates maternal reproduction through LIF. *Nature* **450:** 721–724.

Huttinger-Kirchhof, N., Cam, H., Griesmann, H., Hofmann, L., Beitzinger, M., and Stiewe, T. 2006. The p53 family inhibitor ΔNp73 interferes with multiple developmental programs. *Cell Death Differ.* **13:** 174–177.

Irwin, M., Marin, M.C., Phillips, A.C., Seelan, R.S., Smith, D.I., Liu, W., Flores, E.R., Tsai, K.Y., Jacks, T., Vousden, K.H., et al. 2000. Role for the p53 homologue p73 in E2F-1-induced apoptosis. *Nature* **407:** 645–648.

Jurisicova, A., Rogers, I., Fasciani, A., Casper, R.F., and Varmuza, S. 1998. Effect of maternal age and conditions of fertilization on programmed cell death during murine preimplantation embryo development. *Mol. Hum. Reprod.* **4:** 139–145.

Kaghad, M., Bonnet, H., Yang, A., Creancier, L., Biscan, J.C., Valent, A., Minty, A., Chalon, P., Lelias, J.M., Dumont, X., et al. 1997. Monoallelically expressed gene related to p53 at 1p36, a region frequently deleted in neuroblastoma and other human cancers. *Cell* **90:** 809–819.

Keyes, W.M., Wu, Y., Vogel, H., Guo, X., Lowe, S.W., and Mills, A.A. 2005. p63 deficiency activates a program of cellular senescence and leads to accelerated aging. *Genes & Dev.* **19:** 1986–1999.

Klanrit, P., Flinterman, M.B., Odell, E.W., Melino, G., Killick, R., Norris, J.S., and Tavassoli, M. 2008. Specific isoforms of p73 control the induction of cell death induced by the viral proteins, E1A or apoptin. *Cell Cycle* **7:** 207–215.

Li, Y. and Prives, C. 2007. Are interactions with p63 and p73 involved in mutant p53 gain of oncogenic function? *Oncogene* **26:** 2220–2225.

Lissy, N.A., Davis, P.K., Irwin, M., Kaelin, W.G., and Dowdy, S.F. 2000. A common E2F-1 and p73 pathway mediates cell death induced by TCR activation. *Nature* **5:** 642–645.

Maisse, C., Munarriz, E., Barcaroli, D., Melino, G., and De Laurenzi, V. 2004. DNA damage induces the rapid and selective degradation of the ΔNp73 isoform, allowing apoptosis to occur. *Cell Death Differ.* **11:** 685–687.

Martinez-Delgado, B., Melendez, B., Cuadros, M., Garcia, M.J., Nomdedeu, J., Rivas, C., Fernandez-Piqueras, J., and Benitez, J. 2002. Frequent inactivation of the p73 gene by abnormal methylation or LOH in non-Hodgkin's lymphomas. *Int. J. Cancer* **102:** 15–19.

Matikainen, T., Perez, G.I., Jurisicova, A., Pru, J.K., Schlezinger, J.J., Ryu, H.-Y., Laine, J., Sakai, T., Korsmeyer, S.J., Casper, R.F., et al. 2001. Aromatic hydrocarbon receptor-driven *Bax* gene expression is required for premature ovarian failure caused by biohazardous environmental chemicals. *Nat. Genet.* **28:** 355–360.

McKeon, F. and Melino, G. 2007. Fog of war: The emerging p53 family. *Cell Cycle* **6:** 229–232.

Mills, A.A., Zheng, B., Wang, X.J., Vogel, H., Roop, D.R., and Bradley, A. 1999. p63 is a p53 homologue required for limb and epidermal morphogenesis. *Nature* **398:** 708–713.

Müller, M., Schilling, T., Sayan, A.E., Kairat, A., Lorenz, K., Schulze-Bergkamen, H., Oren, M., Koch, A., Tannapfel, A., and Stremmel, W. 2005. TAp73/ΔNp73 influences apoptotic response, chemosensitivity and prognosis in hepatocellular carcinoma. *Cell Death Differ.* **12:** 1564–1577.

Munarriz, E., Barcaroli, D., Stephanou, A., Townsend, P.A., Maisse, C., Terrinoni, A., Neale, M.H., Martin, S.J., Latchman, D.S., Knight, R.A., et al. 2004. PIAS-1 is a checkpoint

regulator which affects exit from G1 and G2 by sumoylation of p73. *Mol. Cell. Biol.* **24:** 10593–10610.

Murray-Zmijewski, F., Lane, D.P., and Bourdon, J.C. 2006. p53/p63/p73 isoforms: An orchestra of isoforms to harmonise cell differentiation and response to stress. *Cell Death Differ.* **13:** 962–972.

Niikura, Y., Dixit, A., Scott, R., Perkins, G., and Kitagawa, K. 2007. BUB1 mediation of caspase-independent mitotic death determines cell fate. *J. Cell Biol.* **178:** 283–296.

Ohkusu-Tsukada, K., Tsukada, T., and Isobe, K. 1999. Accelerated development and aging of the immune system in p53-deficient mice. *J. Immunol.* **163:** 1966–1972.

Ono, R., Nakamura, K., Inoue, K., Naruse, M., Usami, T., Wakisaka-Saito, N., Hino, T., Suzuki-Migishima, R., Ogonuki, N., Miki, H., et al. 2006. Deletion of Peg10, an imprinted gene acquired from a retrotransposon, causes early embryonic lethality. *Nat. Genet.* **38:** 101–106.

Perez, G.I., Jurisicova, A., Matikainen, T., Moriyama, T., Kim, M., Takai, Y., Pru, J.K., Kolesnick, R.N., and Tilly, J.L. 2005. A central role for ceramide in the aging-related acceleration of apoptosis in the female germ line. *FASEB J.* **19:** 860–872.

Pérez de Castro, I., de Cárcer, G., and Malumbres, M. 2007. A census of mitotic cancer genes: New insights into tumor cell biology and cancer therapy. *Carcinogenesis* **28:** 899–912.

Perez-Losada, J., Wu, D., Delrosario, R., Balmain, A., and Mao, J.H. 2005. p63 and p73 do not contribute to p53-mediated lymphoma suppressor activity in vivo. *Oncogene* **24:** 5521–5524.

Pozniak, C.D., Radinovic, S., Yang, A., McKeon, F., Kaplan, D.R., and Miller, F.D. 2000. An anti-apoptotic role for the p53 family member, p73, during developmental neuron death. *Science* **289:** 304–306.

Pozniak, C.D., Barnabe-Heider, F., Rymar, V.V., Lee, A.F., Sadikot, A.F., and Miller, F.D. 2002. p73 is required for survival and maintenance of CNS neurons. *J. Neurosci.* **22:** 9800–9809.

Pûtzer, B.M., Tuve, S., Tannapfel, A., and Stiewe, T. 2003. Increased ΔN-p73 expression in tumors by upregulation of the E2F1-regulated, TA-promoter-derived ΔN'-p73 transcript. *Cell Death Differ.* **10:** 612–614.

Roman-Gomez, J., Gimenez-Velasco, A., Agirre, X., Castillejo, J.A., Navarro, G., Calasanz, M.J., Garate, L., San jose-Eneriz, E., Cordeu, L., Prosper, F., et al. 2006. CpG island methylator phenotype redefines the prognostic effect of t(12,21) in childhood acute lymphoblastic leukemia. *Clin. Cancer Res.* **12:** 4845–4850.

Steuerwald, N.M., Bermúdez, M.G., Wells, D., Munné, S., and Cohen, J. 2007. Maternal age-related differential global expression profiles observed in human oocytes. *Reprod. Biomed. Online* **14:** 700–708.

Stiewe, T. 2007. The p53 family in differentiation and tumorigenesis. *Nat. Rev. Cancer* **7:** 165–168.

Stiewe, T. and Pûtzer, B.M. 2000. Role of the p53-homologue p73 in E2F1-induced apoptosis. *Nat. Genet.* **26:** 464–469.

Suh, E.K., Yang, A., Kettenbach, A., Bamberger, C., Michaelis, A.H., Zhu, Z., Elvin, J.A., Bronson, R.T., Crum, C.P., and McKeon, F. 2006. p63 protects the female germ line during meiotic arrest. *Nature* **444:** 624–628.

Talos, F., Nemajerova, A., Flores, E.R., Petrenko, O., and Moll, U.M. 2007. p73 suppresses polyploidy and aneuploidy in the absence of functional p53. *Mol. Cell* **27:** 647–659.

Tarin, J.J., Perez-Albala, S., and Cano, A. 2001. Cellular and morphological traits of oocytes retrieved from aging mice after exogenous ovarian stimulation. *Biol. Reprod.* **65:** 141–150.

Thomas, N.S., Ennis, S., Sharp, A.J., Durkie, M., Hassold, T.J., Collins, A.R., and Jacobs, P.A. 2001. Maternal sex chromosome non-disjunction: Evidence for X chromosome-specific risk factors. *Hum. Mol. Genet.* **10:** 243–250.

Toh, W.H., Siddique, M.M., Boominathan, L., Lin, K.W., and Sabapathy, K. 2004. c-Jun regulates the stability and activity of the p53 homologue, p73. *J. Biol. Chem.* **279:** 44713–44722.

Tomasini, R., Mak, T.W., and Melino, G. 2008. The impact of p53 and p73 on aneuploidy and cancer. *Trends Cell Biol.* **18:** 244–252.

Tusher, V.G., Tibshirani, R., and Chu, G. 2001. Significance analysis of microarrays applied to the ionizing radiation response. *Proc. Natl. Acad. Sci.* **98:** 5116–5121.

Tyner, S.D., Ventakachalam, S., Choi, J., Jones, S., Ghebranious, N., Igelmann, H., Lu, X., Soron, G., Cooper, B., Brayton, C., et al. 2002. p53 mutant mice that display early ageing-associated phenotypes. *Nature* **415:** 45–53.

Vousden, K.H. and Lane, D.P. 2007. p53 in health and disease. *Nat. Rev. Mol. Cell Biol.* **8:** 275–283.

Walsh, G.S., Orike, N., Kaplan, D.R., and Miller, F.D. 2004. The invulnerability of adult neurons: A critical role for p73. *J. Neurosci.* **24:** 9638–9647.

Wang, J., Liu, Y.X., Hande, M.P., Wong, A.C., Jin, Y.J., and Yin, Y. 2007. TAp73 is a downstream target of p53 in controlling the cellular defense against stress. *J. Biol. Chem.* **282:** 29152–29162.

Weaver, B.A. and Cleveland, D.W. 2007. Aneuploidy: Instigator and inhibitor of tumorigenesis. *Cancer Res.* **67:** 10103–10105.

Yamamoto, M., Sato, S., Hemmi, H., Uematsu, S., Hoshino, K., Kaisho, T., Takuechi, O., Takeda, K., and Akira, S. 2003. TRAM is specifically involved in the toll-like receptor 4-mediated MyD88-independent signaling pathway. *Nat. Immunol.* **4:** 1144–1150.

Yang, A., Schweitzer, R., Sun, D., Kaghad, M., Walker, N., Bronson, R.T., Tabin, C., Sharpe, A., Caput, D., and Crum, C. 1999. p63 is essential for regenerative proliferation in limb, craniofacial and epithelial development. *Nature* **398:** 714–718.

Yang, A., Walker, N., Bronson, N., Kaghad, M., Oosterwegel, M., Bonnin, J., Vagner, C., Bonnet, H., Dikkes, P., Sharpe, A., et al. 2000. p73-deficient mice have neurological, pheromonal and inflammatory defects but lack spontaneous tumours. *Nature* **404:** 99–103.

Yang, A., Kaghad, M., Caput, D., and McKeon, F. 2002. On the shoulders of giants: p63, p73 and the rise of p53. *Trends Genet.* **18:** 90–95.

Yao, L.J., Zhong, Z.S., Zhang, L.S., Chen, D.Y., Schatten, H., and Sun, Q.Y. 2004. Aurora-A is a critical regulator of microtubule assembly and nuclear activity in mouse oocytes, fertilized eggs, and early embryos. *Biol. Reprod.* **70:** 1392–1399.

Yuen, K.W., Montpetit, B., and Hieter, P. 2005. The kinetochore and cancer: What's the connection? *Curr. Opin. Cell Biol.* **17:** 576–582.

Zaika, A.I., Slade, N., Erster, S.H., Sansome, C., Joseph, T.W., Pearl, M., Chalas, E., and Moll, U.M. 2002. ΔNp73, a dominant-negative inhibitor of wild-type p53 and TAp73, is up-regulated in human tumors. *J. Exp. Med.* **196:** 765–780.

Susceptibility of *Snark*-deficient mice to azoxymethane-induced colorectal tumorigenesis and the formation of aberrant crypt foci

Katsuya Tsuchihara,[1] Tsutomu Ogura,[3] Rumi Fujioka,[1] Satoshi Fujii,[2] Wataru Kuga,[1,4] Marie Saito,[1,4] Takahiro Ochiya,[5] Atsushi Ochiai[2,4] and Hiroyasu Esumi[1,4,6]

[1]Cancer Physiology Project, [2]Pathology Division, Research Center for Innovative Oncology, National Cancer Center Hospital East, 6-5-1 Kashiwanoha, Kashiwa, Chiba 277-8577; [3]Department of Bioinformatics Sciences, Faculty of Pharmaceutical Sciences, Hokuriku University, Kanazawa, Ishikawa 920-1180; [4]Department of Integrated Biosciences, Graduate School of Frontier Sciences, The University of Tokyo, 5-1-5 Kashiwanoha, Kashiwa, Chiba 277-8561; [5]Section for Studies on Metastasis, National Cancer Center Research Institute, Tsukiji, Chuo-ku, Tokyo 104-0045, Japan

(Received October 30, 2007/Revised December 3, 2007/Accepted December 5, 2007/Online publication February 27, 2008)

SNF-1/5′-AMP-activated kinase (AMPK)-related kinase (SNARK) is a member of the AMPK-related kinases. *Snark*$^{+/-}$ mice exhibited mature-onset obesity and related metabolic disorders. Obesity is regarded as a risk factor for colorectal cancer. To investigate whether *Snark* deficiency is involved in tumorigenesis in the large intestine, obese *Snark*$^{+/-}$ mice were treated with a chemical carcinogen, azoxymethane (AOM). The incidences of both adenomas and aberrant crypt foci (ACF) were significantly higher in *Snark*$^{+/-}$ mice than in their wild-type counterparts 28 weeks after the completion of AOM treatment (10 mg/kg/week for 8 weeks). Furthermore, ACF formation was enhanced in *Snark*$^{+/-}$ mice treated with AOM for 2 weeks, suggesting that *Snark* deficiency contributed to the early phase of tumorigenesis. The total number of ACF was correlated with bodyweight in *Snark*$^{+/-}$ and *Snark*$^{+/+}$ mice, suggesting that obesity was a risk factor for colorectal tumorigenesis in this model. However, the correlation coefficient was higher in *Snark*$^{+/-}$ mice. Moreover, AOM-induced ACF formation was also enhanced in preobese *Snark*$^{+/-}$ mice. Together, these findings suggest that AOM-induced tumorigenesis in *Snark*$^{+/-}$ mice was enhanced via obesity-dependent and -independent mechanisms. (*Cancer Sci* 2008; 99: 677–682)

AMP-activated protein kinase is a conserved serine/threonine kinase that acts as a cellular energy sensor. Once cellular ATP is consumed, activated AMPK suppresses anabolic pathways to decrease energy expenditure and activates catabolic pathways to produce ATP.[1] Furthermore, recent studies have implicated AMPK in the regulation of whole-body metabolic homeostasis, including the regulation of food intake and energy expenditure.[2] Based on the similarity of their kinase domains, 14 AMPK-related kinases have been predicted in the human genome.[3,4] SNARK (encoded by the *NUAK2* locus) is the fourth identified AMPK-related kinase.[5] Although several *in vitro* studies have suggested that metabolic stresses as well as genotoxic or osmotic stresses induce SNARK activation, the physiological roles of SNARK remain uncertain.[5–7] We established *Snark*-deficient mice to clarify its *in vivo* function. Heterozygotic mice exhibited an increased bodyweight accompanied with fat deposition, fatty changes of the liver, and increased serum triglyceride concentration. These mice also exhibited hyperinsulinemia, hyperglycemia, and glucose intolerance. These symptoms are similar to those of human type II diabetes mellitus accompanied with obesity (K. Tsuchihara *et al.*, manuscript in preparation, 2008).

Several epidemiological studies and rodent models have addressed the relationship between colorectal tumorigenesis and obesity or obesity-related metabolic disorders.[8–17] We suspected that the metabolic disorders in *Snark*-deficient mice might be correlated with tumorigenesis. Furthermore, SNARK activity is reportedly upregulated under genotoxic stresses in some cell culture systems, suggesting the potential roles of SNARK in cellular stress responses.[6] These findings prompted us to explore the involvement of Snark in colorectal tumor formation in Snark-deficient and wild-type mice treated with AOM, a chemical carcinogen that induces ACF, colorectal adenoma, and adenocarcinoma. We then assessed the chemically induced pre-neoplastic and neoplastic lesions in both obese and preobese *Snark*-deficient mice.

Materials and Methods

Reverse transcription–polymerase chain reaction. Total RNA was extracted from tissues obtained from 3-month-old *Snark*$^{+/-}$ and *Snark*$^{+/+}$ mice using TRIzol Reagent (Invitrogen, Carlsbad, CA, USA). RT was carried out using a High Capacity cDNA Reverse Transcription Kit (Applied Biosystems, Foster City, CA, USA). Quantitative PCR was carried out using TaqMan Gene Expression Assays and the 7500 Fast Real-Time PCR System (Applied Biosystems). The relative abundance of transcripts was normalized to the constitutive expression of mouse *Actb* mRNA.

Generation of *Snark*-deficient mice. To construct the targeting vector for the disruption of the *Snark* gene, a neomycin-resistance gene driven by the herpes simplex virus (HSV) thymidine kinase promoter (tk-Neo) was substituted for exon 1 of the mouse *Nuak2* locus, which encodes the *Snark* gene. The diphteria toxin gene was inserted into the targeting vector for negative selection (Fig. 1b). J1 mouse ES cells from 129SVJ mice were electroporated with the linearized targeting vector and cultured in the presence of 300 μg/mL G418 for 14 days. G418-resistant ES cells were screened for homologous recombination using PCR. Correctly targeted ES clones were verified using a Southern blot analysis. Information regarding the PCR primers and Southern blot probes is available on request. Two ES clones containing the *Snark*-disrupted allele were obtained. One of the positive clones was injected into C57BL/6 J blastocysts to generate chimeric mice. After successful germline transmission, the F_1 offspring were back-crossed to C57BL/6 J mice for six generations. Offspring from the six-generation heterozygous intercrosses were used for the experiments. Mouse embryonic fibroblasts derived from E13.5 embryos were prepared according to standard procedures. All of the mice were maintained in plastic cages with hardwood chip bedding in an airconditioned room with a 12:12 h L:D cycle and were given food (Oriental CRF-1; Oriental Yeast, Tokyo, Japan), irradiated with 30 Gy gamma

[6]To whom correspondence should be addressed. E-mail: hesumi@east.ncc.go.jp
Abbreviations: ACF, aberrant crypt foci; AMPK, 5′-AMP-activated kinase; AOM, azoxymethane; ES, embryonic stem; PBS, phosphate-buffered saline; PCR, polymerase chain reaction; RT, reverse transcription; SNARK, SNF-1/AMPK-related kinase.

doi: 10.1111/j.1349-7006.2008.00734.x

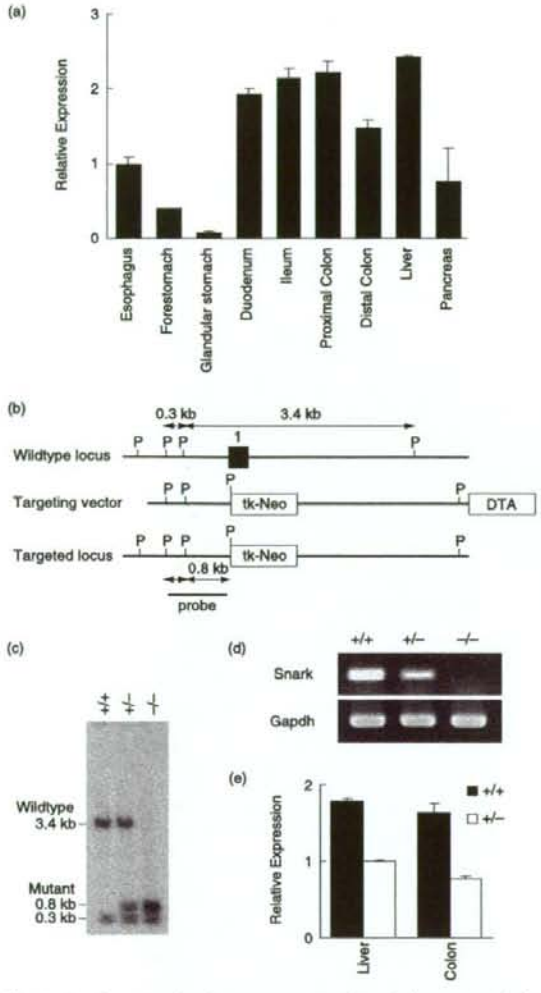

Fig. 1. *Snark* expression in mouse gastrointestinal tract and the generation of *Snark*-deficient mice. (a) Relative quantitative (RQ) reverse transcription–polymerase chain reaction (RT-PCR) quantification of *Snark* transcripts normalized for *Actb* in adult C57BL/6 J mouse tissues of the digestive organs. The results are expressed as the mean value ± SD ($n = 4$) relative to the expression level in the esophagus. (b) Schematic representations of the wild-type *Snark* locus, targeting vector, and targeted allele. Exon 1 is indicated by a filled box. The 5′ probe used for Southern hybridization is shown. P, *Pst*I site. (c) Southern blot analysis of genomic DNA from $Snark^{-/-}$, $Snark^{+/-}$, and $Snark^{+/+}$ mouse embryo fibroblasts (MEF) hybridized to the 5′ probe shown (b). (d) RT-PCR analysis of total RNA from $Snark^{-/-}$, $Snark^{+/-}$, and $Snark^{+/+}$ MEF. (e) RQ RT-PCR analysis of total RNA from $Snark^{+/-}$ and $Snark^{+/+}$ liver and large intestine. The results are expressed as the mean value ± SD ($n = 3$) relative to the expression level in the $Snark^{+/-}$ liver. DTA, diphteria toxin A chain; Gapdh, glyceraldehyde-3-phosphate dehydrogenase.

rays, and given filtered tap water *ad libitum*. The study was approved by the Institutional Ethics Review Committee for animal experiments at the National Cancer Center Hospital East.

Azoxymethane treatment. AOM (Sigma-Aldrich, St Louis, MO, USA) was dissolved in PBS at a concentration of 1 mg/mL. For the long-term experiment, 6-month-old male $Snark^{+/-}$ and $Snark^{+/+}$ mice were injected with 10 mg AOM per kg bodyweight intraperitoneally once a week for 8 weeks (eight administrations in total). The mice were then killed 28 weeks after the last AOM injection. For the short-term experiment, 6-month-old or 4-week-old $Snark^{-/-}$, $Snark^{+/-}$, and $Snark^{+/+}$ male mice were injected with 10 mg AOM per kg bodyweight intraperitoneally once a week for 2 or 4 weeks, respectively, and were then killed 1 week after the final AOM administration.

Aberrant crypt foci assay. Food was withheld from the mice for 16 h prior to dissection. The dissected colons were opened longitudinally, rinsed with PBS, and fixed in 4% neutral buffered formalin for 24 h. After fixation, the specimens were dipped in 0.2% methylene blue and examined using light microscopy. Formalin-fixed and paraffin-embedded sections of the macroscopic tumors were prepared using standard procedures and were examined after hematoxylin–eosin staining.

Immunohistochemistry. Tissue sections were deparaffinized and exposed to 3% hydrogen peroxide for 15 min to block endogenous peroxidase activity. For heat-induced epitope retrieval, the sections were placed in a 0.01 M citrate buffer and heated at 95°C using a microwave for 20 min. The non-specific binding was blocked by preincubation with 2% normal swine serum in PBS (blocking buffer) for 60 min at room temperature. Individual slides were then incubated overnight at 4°C with a monoclonal rat antimouse Ki-67 antigen antibody (clone TEC-3; Dako, Glostrup, Denmark) at a dilution of 1:50 in blocking buffer. The slides were washed with PBS, then incubated with Histofine Mousestain kit (Nichirei, Tokyo, Japan) for 45 min at room temperature. After extensive washing with PBS, the color reaction was developed in 2% 3,3′-diaminobenzidine in 50 mM Tris-buffer (pH 7.6) containing 0.3% hydrogen peroxide for 5–10 min. The sections were then counterstained with Meyer's hematoxylin, dehydrated, and mounted.

Assessment of metabolic parameters. Serum glucose, triglyceride, and free fatty acid levels were determined using the glucose CII-test, triglyceride E-test, and NEFA-C-test (Wako Pure Chemical Industries, Osaka, Japan), respectively.

Statistical analysis. Data were analyzed using the Mann–Whitney *U*-test for statistical significance. *P*-values were considered significant if less than 0.05. The correlation coefficient was measured using Spearman's rank correlation test. *P*-values were considered significant if less than 0.05.

Results

Snark expression in mouse gastrointestinal tract and generation of *Snark*-deficient mice. To examine the expression profile of *Snark* in the mouse gastrointestinal tract, quantitative RT-PCR was carried out using total RNA from 3-month-old C57BL/6 mice. The expression level of Snark in the small and large intestines were comparable to that in the liver, in which *Snark* expression was confirmed in a previous study (Fig. 1a).[5]

To evaluate Snark function *in vivo*, we established Snark-deficient mice (Fig. 1b,c). F_1 heterozygous ($Snark^{+/-}$) mice with mixed background were backcrossed to the C57B6/J strain for six generations. Sixth-generation $Snark^{+/-}$ mice were intercrossed to generate animals homozygous for the mutant *Snark* allele ($Snark^{-/-}$). RT-PCR analysis of $Snark^{-/-}$ mouse embryo fibroblasts isolated on embryonic day 13.5 showed that *Snark* mRNA expression was completely abolished by the biallelic mutation at the *Snark* locus, whereas the hemiallelic mutation reduced *Snark* expression (Fig. 1d). The expression of *Snark* was reduced in the liver and large intestine of adult $Snark^{+/-}$ mice (Fig. 1e). The biallelic mutation of *Snark* was lethal after embroyonic day 16.5; $Snark^{-/-}$ embryos frequently exhibited excencephaly, and less than 10% of the $Snark^{-/-}$ mice were born. Meanwhile, $Snark^{+/-}$ mice were viable and were born at the expected Mendelian ratio (Table 1).

doi: 10.1111/j.1349-7006.2008.00734.x

Table 1. Embryonic lethality of *Snark*$^{-/-}$ mice

Time	-/-		+/-		+/+	
	n	%	*n*	%	*n*	%
E12.5†	2‡	18§	6‡	55§	3‡	27§
E14.5†	6‡	25§	13‡	54§	5‡	21§
E16.5†	12‡	22§	27‡	48§	17‡	30§
P21*	6‡	2§	191‡	62§	110‡	36§

†Embryonic day at the time of genotyping of the embryos. *Post-delivery day at the time of genotyping of the pups. ‡Number of the embryos or pups with each genotype. §Percentage of the embryos or pups with each genotype.

Presence of metabolic disorders in AOM-treated mature *Snark*$^{+/-}$ mice. To evaluate the relevance of *Snark* deficiency in colorectal tumorigenesis, mature (6 months old) *Snark*$^{+/-}$ and *Snark*$^{+/+}$ mice were treated with 10 mg per kg bodyweight AOM intraperitoneally for 8 weeks and killed 28 weeks thereafter. The total dose of AOM was 2.80 ± 0.25 mg for the *Snark*$^{+/-}$ mice and 2.58 ± 0.17 mg for the *Snark*$^{+/+}$ mice. The bodyweights of the *Snark*$^{+/-}$ mice were higher than those of the *Snark*$^{+/+}$ mice at the start of the experiment, and this difference became more pronounced at the end of the experiment (Table 2). The AOM-treated mice did not show any unusual signs during the experimental period with the exception of two *Snark*$^{+/-}$ mice that exhibited bodyweight loss and rough fur during the last 2 weeks of the experimental period. In these mice, huge tumors occupied and obstructed their colons. The bodyweight loss and the rough fur might have been caused by malnutrition as a result of the intestinal obstruction.

The metabolic parameters of the AOM-treated mice (including the two mice with emaciation) were examined. The serum glucose and triglyceride concentration were higher in the *Snark*$^{+/-}$ mice, whereas the free fatty acid concentration was lower compared with the levels in the *Snark*$^{+/+}$ mice (Table 2).

Susceptibility of mature *Snark*$^{+/-}$ mice to AOM-induced tumorigenesis. Six of the 12 *Snark*$^{+/-}$ mice (including the two mice with emaciation) and 3 out of 12 *Snark*$^{+/+}$ mice harbored macroscopic tumors in their large intestines (Table 2). No spontaneous colorectal tumors were detected in age-matched or older untreated mice of either genotypes to date (10 *Snark*$^{+/-}$ mice and eight *Snark*$^{+/+}$ mice, data not shown). Although the individual tumor sizes were similar in the *Snark*$^{+/-}$ and *Snark*$^{+/+}$ mice, the frequency of multiple tumors was higher in the *Snark*$^{+/-}$ mice: five out of six tumor-harboring *Snark*$^{+/-}$ mice had multiple (two to four) tumors, whereas all three *Snark*$^{+/+}$ mice had single tumors (Table 2). All of the tumors that developed in the *Snark*$^{+/-}$ and *Snark*$^{+/+}$ mice appeared to be exophytic rounded or flattened polyps projecting into the intestinal lumen. Pathologically, these tumors were composed of tubules formed by enterocytes with moderate cytological atypia and had not invaded the submucosal layer (Fig. 2a). These tumors were diagnosed as tubular adenomas.[18] Adenocarcinoma was not detected in any of the examined specimens. No obvious tumors were seen in any other organs, including the liver and lungs. Cell proliferation in non-tumorous and adenomatous epithelia was estimated using Ki-67 staining. No significant differences were observed between the *Snark*$^{+/-}$ and *Snark*$^{+/+}$ mice (Table 2).

Susceptibility of mature *Snark*$^{+/-}$ mice to AOM-induced ACF formation. At least one ACF was detected in all of the mice of both genotypes (Figs 2b,3a; Table 2). The mean number of ACF per total colon (from the anal verge to the ileocecal junction) was 6.92 ± 1.09 in the *Snark*$^{+/+}$ mice, whereas that in the *Snark*$^{+/-}$ mice was approximately three times higher (19.42 ± 1.76). The mean numbers of aberrant crypts per focus were 2.37 ± 0.21 in the *Snark*$^{+/-}$ mice and 1.92 ± 0.20 in the *Snark*$^{+/+}$ mice (Table 2). Figure 3a shows the distribution of ACF with multiple crypts for each genotype. The percentages of ACF with more than three crypts were 39.09 ± 8.31% in the *Snark*$^{+/-}$ mice and 25.05 ± 7.66% in the *Snark*$^{+/+}$ mice ($P = 0.025$), whereas the percentages of ACF with more than four crypts were 19.97 ± 6.40% in the *Snark*$^{+/-}$ mice and 8.87 ± 5.77% in the *Snark*$^{+/+}$ mice ($P = 0.022$). Six-month-old *Snark*$^{+/-}$ and *Snark*$^{+/+}$ mice were treated with AOM for 2 weeks and the animals' colons were examined for ACF 3 weeks after the first AOM administration. Three of the five *Snark*$^{+/+}$ mice did not have any ACF, whereas at least four ACF were found in five out of five *Snark*$^{+/-}$ mice. The mean number of ACF per ACF-bearing colon was 6.60 ± 1.69 in *Snark*$^{+/-}$ mice and 2.00 ± 1.00 *Snark*$^{+/+}$ mice (Table 3).

Table 2. Bodyweight, serum parameters, and colorectal lesions induced by long-term azoxymethane (AOM) treatment in *Snark*$^{+/+}$ and *Snark*$^{+/-}$ mice

Genotype	+/+	+/-
Number of animals	12	12
Age (months)†	6	6
Age (months)‡	13	13
AOM administration (weeks)	8	8
Mean total dose of AOM (mg)	2.58 ± 0.17	2.80 ± 0.25
Bodyweight (g)†	31.33 ± 1.40	34.08 ± 1.63§§
Bodyweight (g)‡	34.07 ± 1.80	37.67 ± 1.80††
Blood glucose (mg/dL)‡	106.03 ± 9.46	134.38 ± 17.90††
Serum triglyceride (mg/dL)‡	44.80 ± 8.17	61.07 ± 14.02§§
Serum free fatty acid (mEq/L)‡	0.76 ± 0.12	0.58 ± 0.06§§
Incidence of adenoma¶	3/12	6/12
Mean number of tumors/ tumor bearing mice	1.00 ± 0	2.00 ± 0.58§§
Mean size of adenoma (mm)	5.66 ± 1.22	4.65 ± 0.55
Ki-67 positivity in adenomatous epithelia (%)	28.66 ± 7.02	25.61 ± 5.77
Ki-67 positivity in non-tumorous epithelia (%)	10.04 ± 2.57	10.65 ± 2.60
Incidence of aberrant crypt foci¶	12/12	12/12
Mean number of foci/colon	6.92 ± 1.09	19.42 ± 1.76††
Mean number of aberrant crypts/focus	1.92 ± 0.20	2.37 ± 0.21††

†Values at the time of AOM administration. ‡Values at the time of dissection. ¶Number of mice with adenoma/total mice. ¶Number of mice with aberrant crypt foci/total mice. ††,‡‡,§§Significantly different from the corresponding values in *Snark*$^{+/+}$ mice at levels of $P < 0.01$, $P < 0.02$, and $P < 0.05$, respectively.

Correlation of ACF incidence with bodyweight in AOM-treated mice. A significant correlation between bodyweight and the number of ACF was observed in the *Snark*$^{+/-}$ mice ($\rho = 0.677$, $P = 0.0248$). Although the correlation coefficient and significance were less than those for *Snark*$^{+/-}$ mice, the *Snark*$^{+/+}$ mice also exhibited a correlation between bodyweight and the number of ACF ($\rho = 0.558$, $P = 0.0444$). No significant correlations between the number of ACF and the serum glucose, triglyceride, or free fatty acid concentrations were observed.

Obesity-independent contribution of *Snark* deficiency to ACF formation. To evaluate the obesity-independent contribution of *Snark* deficiency to ACF formation, preobese 4-week-old *Snark*$^{-/-}$, *Snark*$^{+/-}$, and *Snark*$^{+/+}$ mice were treated with AOM for 4 weeks (Table 3). At the end of the AOM treatment, no significant differences in bodyweight were seen among the three genotypes. The incidences of ACF were five out of five, six out of six, and four out of five in the *Snark*$^{-/-}$, *Snark*$^{+/-}$, and *Snark*$^{+/+}$ mice, respectively. Furthermore, the number of ACF was higher